AFRL-AFOSR-VA-TR-2016-0091

(BRI) Direct and Inverse Design Optimization of Magnetic Alloys with Minimized Use of Rare Earth Elements

George Dulikravich
FLORIDA INTERNATIONAL UNIVERSITY

02/02/2016
Final Report

Air Force Research Laboratory
AF Office Of Scientific Research (AFOSR)/ RTB1
Arlington, Virginia 22203
Air Force Materiel Command

REPORT DOCUMENTATION PAGE

Form Approved
OMB No. 0704-0188

1. REPORT DATE *(DD-MM-YYYY)*	2. REPORT TYPE	3. DATES COVERED *(From - To)*
01-20-2016	**FINAL PERFORMANCE REPORT**	**09/01/2012 – 31/10/2015**

4. TITLE AND SUBTITLE
(BRI) Direct and Inverse Design Optimization of Magnetic Alloys with Minimized Use of Rare Earth Elements

5a. CONTRACT NUMBER

5b. GRANT NUMBER
FA9550-12-1-0440

5c. PROGRAM ELEMENT NUMBER

6. AUTHOR(S)
Prof. George S. Dulikravich
Department of Mechanical and Materials Engineering, Room 3462
Florida International University
10555 West Flagler Street, Miami, Florida 33174
(305) 348-7016 phone

5d. PROJECT NUMBER

5e. TASK NUMBER

5f. WORK UNIT NUMBER

7. PERFORMING ORGANIZATION NAME(S) AND ADDRESS(ES)
Florida International University
Office of Research and Economic Development
MARC building, Room 430
11200 SW 8t Street, Miami, FL 33199
(305) 348-2494 phone

8. PERFORMING ORGANIZATION REPORT NUMBER
FIU-AFOSR-800002123-1

9. SPONSORING / MONITORING AGENCY NAME(S) AND ADDRESS(ES)
AFOSR - Air Force Office of Scientific Research
Dr. Ali Sayir, Program Mngr./Aerospace Materials for Extreme Environments
875 North Randolph Street, Suite 325, Room 3026
Arlington, VA 22203-1768
(703) 696-7236 phone

10. SPONSOR/MONITOR'S ACRONYM(S)
AFOSR

11. SPONSOR/MONITOR'S REPORT NUMBER(S)

12. DISTRIBUTION / AVAILABILITY STATEMENT
Distribution A – Approved for Public Release

13. SUPPLEMENTARY NOTES
The subcontract on this grant was North Carolina State University, Dept. of Materials Science and Eng., Raleigh, NC (Profs. Justin Schwartz and Carl C. Koch). Their team performed all manufacturing and experimental measurements.

14. ABSTRACT

This project deals with the industry-wide need for developing a new generation of high strength magnetic materials with minimal use of rare earth elements. We studied an extended AlNiCo family of magnetic alloys with 8 alloying elements and no rare earths. Existing theoretical formulations and accompanying software can predict only certain physical properties of such materials and they are currently limited to at most three alloying elements. We used advanced semi-stochastic algorithms for constrained multi-objective optimization in combination with experimental testing and verification of candidate alloys. These optimization algorithms allow for concentrations of a large number of alloying elements to be optimized so that several physical properties of the alloy are simultaneously extremized in a Pareto sense. This approach was successful in evolving chemical concentrations of an initial set of candidate alloys with negligible magnetic properties into concentrations of alloys with properties comparable to commercially available AlNiCo alloys. Pattern recognition statistical algorithms were also used to elucidate relationships among different alloying elements and each of the desired magnetic properties of the alloys. Sensitivity analysis of the variation of concentrations of each of the alloying elements revealed that some of the alloying elements have practically negligible influence on the magnetic properties of the AlNiCo type alloys. Research is recommended on determining which of the alloying elements could be replaced with small amounts of rare earth elements and optimizing thermal treatment protocols for higher magnetic performance of such alloys.

15. SUBJECT TERMS
Magnetic alloys; AlNiCo alloys; materials science; materials design; alloys design; multi-objective optimization;

16. SECURITY CLASSIFICATION OF:			17. LIMITATION OF ABSTRACT	18. NUMBER OF PAGES	19a. NAME OF RESPONSIBLE PERSON
UNCLASSIFIED					**George S. Dulikravich, PhD**
a. REPORT	b. ABSTRACT	c. THIS PAGE	**UU**	**50**	19b. TELEPHONE NUMBER *(include area code)*
U	**U**	**U**			**(305) 348-7016**

Standard Form 298 (Rev. 8-98)
Prescribed by ANSI Std. Z39.18

FINAL PERFORMANCE REPORT

Submitted to: **technicalreports@afosr.af.mil**

Contract/Grant Title:

Direct and Inverse Design Optimization of Magnetic Alloys with Minimized Use of Rare Earth Elements

Contract/Grant #: **FA9550-06-1-0170**

Reporting Period: **1 September 2012 to 30 October 2015**

Name of Principal Investigator:

Prof. George S. Dulikravich, Ph.D.
Department of Mechanical and Materials Engineering, EC3462
Florida International University
10555 West Flagler Street
Miami, Florida 33174
305-348-7016 (Phone) 305-348-1932 (FAX) dulikrav@fiu.edu (E-mail)

Names of Co-Investigators:

Prof. Carl C. Koch, PhD and Prof. Justin Schwartz, PhD
Department of Materials Science and Engineering, North Carolina State University, Campus Box 7907, Raleigh, NC 27695-7907
cckoch@ncsu.edu justin_schwartz@ncsu.edu

Final Program Manager:

Ali Sayir, PhD, DAF, ACER Fellow
Program Officer / RTD-Aerospace Materials for Extreme Environments
Air Force Office of Scientific Research
875 North Randolph Street, Suite 325, Room 3026
Arlington, Virginia 22203
(703) 696-7236 Phone & (703) 696-7320 Fax
ali.sayir.2@us.af.mil

Changes in research objectives, if any:	**None**
Change in AFOSR program manager, if any:	**None**
Extensions granted or milestones slipped, if any**:**	**None**
Include any new discoveries, inventions, or patent disclosures:	**None**

Appendix A: The chemical compositions of 180 alloys that were manufactured and tested
Appendix B: (compressed bundle FA955-12-1-0440-Appendix A-presentations
Appendix C: (compressed bundle FA9550-12-1-0440-Appendix B-publications)

Submission Date: **January 20, 2016**

DIRECT AND INVERSE DESIGN OPTIMIZATION OF MAGNETIC ALLOYS WITH MINIMIZED USE OF RARE EARTH ELEMENTS

EXECUTIVE SUMMARY

Contents	2
Statement of Objectives	2
Summary of Significant Results	3
Background and Basics of Magnetism	3
A Concept of Iterative Computational-Experimental Design of Alloys	8
Summary of Multi-Objective Optimization Concepts and Metamodels	9
A Step-by-Step Iterative Design of Magnetic Alloys	10
Summary of Experimental Work Performed by a Sub-Contractor (NCSU) Team	11
Results of the Combined Computational-Experimental Iterative Design	15
Results of Statistical Methods Used to Find Trends and Chemistry-Properties Relations	21
Thermodynamic Analysis	34
Discussion	36
Recommendations for Future Research	37
Acknowledgements	38
References	38
Appendix A: Chemical compositions of 180 alloys that were manufactured and tested	42
List of Publications, Presentations and PhD Degrees Awarded Resulting from This Project	47

Statement of Objectives

A novel methodology was proposed for predicting concentration of each of the alloying elements in magnetic alloys so that the new alloys will have simultaneously maximized:

- energy density (BH_{max})
- magnetic remanence (Br)
- intrinsic coercivity (H_c)

while minimizing the concentration of rare earth elements and other expensive elements.

Computational effort on this project was to be performed at Florida International University.

Experimental effort was to be contracted and performed at North Carolina State University.

The proposed optimization method is based on combining NCSU's experimentally obtained multiple properties of the magnetic alloys and FIU's computational hybrid multi-objective constrained optimization algorithms augmented with modeFrontier optimization software, response hypersurface-based metamodels and a modified version of a method of Indirect Optimization based upon Self-Organization. These optimization algorithms allow for concentrations of a large number of alloying elements to be optimized so that several physical properties of the alloy are simultaneously either minimized or maximized, while satisfying a finite number of equality and inequality constraints. During the iterative computational design process at FIU, optimal chemical concentrations of a small set of new magnetic alloys will be periodically predicted. These optimized alloys will then be manufactured and experimentally evaluated for their multiple physical properties at NCSU in order to continuously verify the accuracy of the entire design methodology. This approach will result in a Pareto optimal set of chemical concentrations of alloying elements that will produce the best tradeoff magnetic alloy compositions. This design method enables significant minimization of the number of expensive and time-consuming

experimental evaluations. The proposed research will result in a robust, rigorous and affordable tool for the design optimization of magnetic alloys that use either minimum or none of the rare earth elements and that are unattainable by any other means in existence at the present time.

Summary of Significant Results

This work effectively demonstrated and confirmed the validity of a novel approach to design and optimization of rare-earth free magnetic materials for targeted properties by using various computational and statistical tools in combination with a relatively small number of experimental confirmations. The focus of research during this three-year effort was on multi-objective design optimization of proper concentrations of eight alloying elements constituting a broader family of AlNiCo type alloys that are known to retain their magnetic properties at elevated temperatures and that are valued for their strong anti-corrosive property, ductility and tensile strength. The objectives were to simultaneously maximize (in the Pareto-optimality sense) three of the most important magnetic properties of such alloys: magnetic energy density, magnetic coercivity and magnetic remanence. Initial compositions of candidate alloys were generated using a quasi-random sequence generation algorithm. These randomly generated alloy compositions were then manufactured and experimentally evaluated for the desired magnetic properties. Response surface methodology approach was used to develop meta-models to efficiently link chemistry of these alloys with values of their macroscopic properties. The most accurate meta-models were used for multi-objective optimization of desired properties by utilizing various evolutionary approaches. It was demonstrated that the proposed alloy design methodology is able to successfully and rapidly recover from the initial flaws resulting from random experimentation, which would have been impossible when using standard alloy design methods.

Various statistical tools and pattern recognition techniques were used to determine patterns and correlations within the created dataset. Pareto-optimized candidate alloys were experimentally validated and used to improve the accuracy of the response surface generation. Multi-objective optimizers were then used on these response surfaces to find the next generation of Pareto-optimal alloys. Results over the cycles show significant experimentally verified improvement in the properties of these alloys. Specifically, the resulting Pareto-optimized alloy compositions rival macroscopic magnetic properties of commercial AlNiCo alloys, but have different chemical concentrations, thus, suggesting that optimization algorithms are capable of exploring yet unexplored domains of the design space. Sensitivity analysis also revealed that certain alloying elements have negligible influence on magnetic properties of the alloy and could be replaced by some of the affordable and readily available rare-earth elements. Finally, besides its robustness, versatility and computational efficiency, this magnetic alloy design methodology has an implicit continuous experimental verification built in and it requires minimal number of candidate alloys to be manufactured and tested, thus, making general alloy design affordable and fully verified.

Background and Basics of Magnetism

Rare Earth Element (REE) based magnets [1] have a very high magnetic energy density ($(BH)_{max}$). This means that it is possible to synthesize smaller magnets while maintaining the superior magnetic properties. These magnets also have higher coercivity (H_c), making it difficult to demagnetize under external magnetic fields. Neodymium magnets are the strongest available magnets in this family. However, Nd-Fe-B (Neodymium-Iron-Boron) performs the best up to 150 °C. From 150 °C to 350 °C, Sm-Co (Samarium-Cobalt) magnets are used. These magnets usually need a protective coating in order to prevent corrosion. REE-based magnetic materials are essential

in electric cars, in wind turbine electric generators, and any high-efficiency electric devices requiring magnetic fields. Hence, REEs are classified as strategic materials [2] determining which national economies will survive and prosper in the post-combustion-engine era. Most of the rare earth elements used for synthesizing these magnets are located in China and the Russian federation. Due to depleting resources and stringent trade rules from the suppliers, it is important to look at other options to synthesize these magnets [3].

AlNiCo magnets [4] are permanent magnetic alloys based on the Fe-Co-Ni-Al system without REEs. AlNiCo magnets have high B_r values, comparable to REE magnets. AlNiCo magnets have lower H_c values and can be demagnetized in the presence of an external magnetic field. Low H_c can be helpful as these magnets can be easily magnetized to saturation. A high B_r and low H_c value can be properly exploited to cast this magnet in complex shapes while magnetizing it in the production heat treatment stages. AlNiCo magnets possess excellent corrosion resistance and high-temperature stability. These are the only magnets that are stable up to 800 °C (Curie temperature). Above-mentioned properties have been successfully exploited by researchers in the past and are a perfect choice for military and automotive sensor applications. Thus, any improvement in the existing properties of AlNiCo alloys will be helpful in covering the gap between the magnetic properties achieved by AlNiCo and REE based magnets.

In the present research work, a novel approach is presented for creating computational tools for design and multi-objective optimization of permanent magnetic alloys. The proposed research combines a number of numerical design optimization algorithms with several concepts from artificial intelligence and experimentally evaluated desired properties of an affordable set of candidate alloys. These alloys were further screened by various statistical tools in order to determine any specific trend in the data. This information will be helpful to the research community in developing a material knowledge base for the design of new alloys for targeted properties.

At present, researchers around the globe are working on designing magnetic alloys that will be able to cover the gap between the properties achieved by AlNiCo magnets and the rare-earth magnets, basically by adding a small amount of those rare-earth elements that are less critical in the sense of supply [5,6]. Sellmyer et al. [7] worked on a few rare-earth free alloys. Zhou et al. [8] manufactured a few commercial AlNiCo alloys to demonstrate the scope of improvement in this field. The difference between the theoretically calculated and the experimentally measured properties was quite large for both ($(BH)_{max}$) and H_c. Thus, random experimentation may prove to be both expensive and time-consuming.

Designing a new alloy system is a challenging task mainly due to a limited experimental database. In order to develop a reliable knowledge base [9] for design of new alloys, one needs to focus on determining various correlations (composition-property, property-property, and composition-composition) from the available databases (simulated and experimental). This information can be coupled with the theoretical knowledge (atomistic and continuum based theories) to develop the knowledge base. Integrated Computational Materials Engineering (ICME) approach [10] and materials genome initiative highlighted the importance and growing application of computational tools in the design of new alloys. In recent years, various data-driven techniques combined with evolutionary approaches [11,12] have been successfully implemented in the direct alloy design. The alloy design optimization method presented in this document was developed by the Principal Investigator during the previous decade and applied to design optimization of H-type steels, Ni

based superalloys, Hf based bulk metallic glasses, Al based alloys and Ti based alloys [13-23]. It is capable of exploring new alloys with chemical concentrations outside of the initial experimental data set. Dulikravich also demonstrated an inverse alloy design method [24] where multiple macroscopic properties of an alloy family are specified. The corresponding ranges of concentrations of each of the alloying elements are then determined that will produce the specified magnitudes of macroscopic properties. Improving thermodynamic databases such as Thermocalc [25] for alloy development has also been pursued. Jha et al. [26,27] demonstrated the scope of use of these databases for designing Ni-based superalloy and Rettig et al. [28] performed a few experiments to confirm his findings. Data mining approaches such as Principal Component Analysis (PCA) and Partial Least Square (PLS) regression have also been successfully used in designing new alloys [29,30]. Additionally, various machine-learning algorithms have been used to address a vast range of problems in materials design [31,32]. These applications demonstrate the diversity and efficacy of application of computational tools for materials design.

Mishima in Japan [4] first discovered AlNiCo magnets in 1931. Initially, it belonged to the Fe-Co-Ni-Al quaternary system. Magnetic properties in these magnets were attributed to the presence of a two-phase system, α_1 and α_2, of Body Centered Cubic (BCC). It was later observed that separation of α_1 and α_2 phases is due to a metallurgical phenomenon popularly known as spinodal decomposition. Phase α_1 is Fe-Co rich ferromagnetic phase and α_2 is Ni-Al rich phase. Phases α_1 and α_2 are stable up to 850 ºC that is just below the Curie temperature, which is about 860 ºC. Above 850 ºC, Face Centered Cubic (FCC) γ phase begins to appear and it was observed in a few samples [33]. Gamma phase must be avoided, as it is detrimental for magnetic properties. Various attempts (such as modification of heat treatment protocol and addition of various alloying elements) have been made to stabilize the magnetic α_1 and α_2 phases and simultaneously eliminate or reduce the amount of γ phase. In the past few decades, (especially after the discovery of powerful REE-based magnets in 1980's), there has been limited research on AlNiCo magnets. Recent rise in prices of rare earth elements led to the search for rare-earth free magnets. In recent years, AlNiCo magnets are again a popular choice for research mainly due to their proven high-temperature stability and related properties at an affordable cost [34].

Currently, AlNiCo alloys are not limited to quaternary systems and may contain eight or more elements [4,11,12,27,35]. In this work, we selected 8 elements namely Iron (Fe), Cobalt (Co), Nickel (Ni), Aluminum (Al), Titanium (Ti), Hafnium (Hf), Copper (Cu) and Niobium (Nb). Variable bounds of these elements have been tabulated in Table 1. From both experimental as well as the modeling point of view, it will be helpful to discuss the role of these alloying elements. This information can be utilized to select meta-model for targeted properties. This will be helpful in developing a knowledge base for discovery of new materials and/or improving properties of existing materials.

As shown in Figure 1, magnetic energy density ($(BH)_{max}$) is mathematically the area of the largest rectangle that can be inscribed in the second quadrant of B-H curve [36]. Since, H_c and B_r are conflicting; one has to sacrifice on one of these properties to improve the other property. Therefore, in order to increase $(BH)_{max}$, one needs to optimize H_c and B_r.

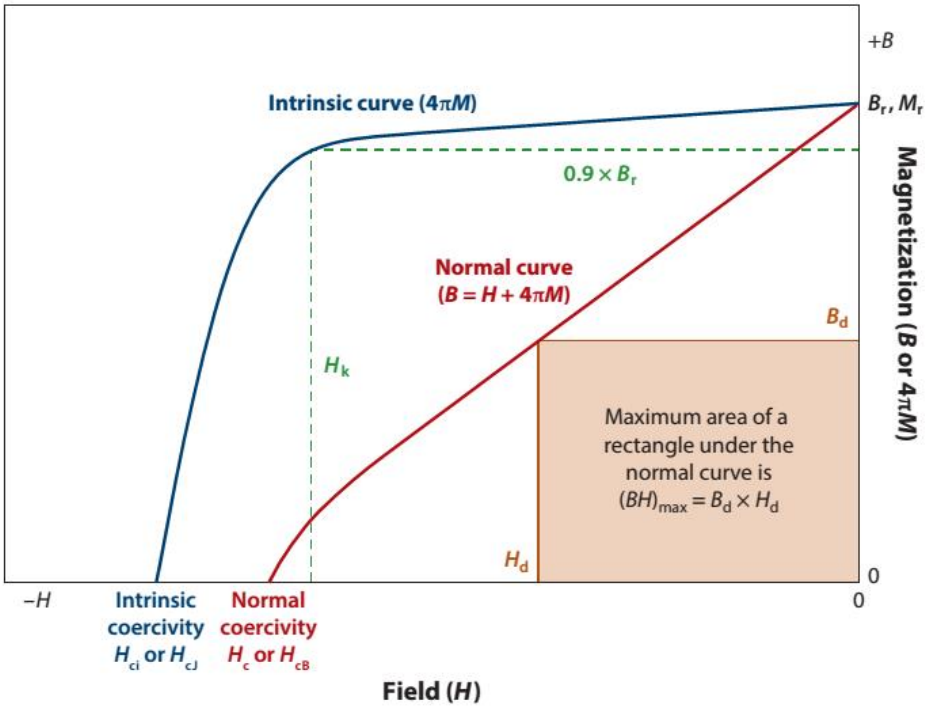

Fig. 1 B-H curve: shows relation between Hc, Br and $((BH)_{max})$ [36].

It is helpful at this point to recall the basic symbolism and relations used in magnetism.

$\underline{\mathbf{B}} = \mu_0(\underline{\mathbf{H}} + \underline{\mathbf{M}})$	magnetic flux density, kg A^{-1} s^{-2}
$\underline{\mathbf{H}} = \frac{\underline{\mathbf{B}}}{\mu_0} - \underline{\mathbf{M}}$	magnetic field intensity in a magnetizable medium, A m^{-1}
$\mathbf{M}_m$	magnetization per unit volume due to rotation of charged particles, A m^{-1}
$\mathbf{M}_p$	intrinsic or natural magnetization per unit volume, A m^{-1}
$\mathbf{M}=\mathbf{M}_m+\mathbf{M}_p$	total magnetization per unit volume, A m^{-1}
$\mu_m = \frac{\mu_0 \mu}{\mu - \mu_0}$	magnetization magnetic permeability, kg m A^{-2} s^{-2}
μ	magnetic permeability coefficient, kg m A^{-2} s^{-2}
$\mu_0 = 4\pi \times 10^{-7}$	magnetic permeability coefficient of vacuum, kg m A^{-2} s^{-2}
$\mu_r = \mu / \mu_0$	relative magnetic permeability
$\chi_m = \mu_r - 1$	magnetic susceptibility

The magnetization vector, ***M***, and magnetic field vector, ***B***, are often combined to form the *magnetic field strength* vector, ***H*** [37].

$$\boldsymbol{B} = \mu_o(\boldsymbol{H} + \boldsymbol{M}_m + \boldsymbol{M}_p) = \mu_o(\boldsymbol{H} + \boldsymbol{M}) \quad (1)$$

Hence

$$\boldsymbol{H} = \frac{\boldsymbol{B}}{\mu_o} - \boldsymbol{M} \quad (2)$$

For linear materials that do not contain ordered paramagnetic ions, magnetization, ***M,*** is typically related linearly to magnetic field strength, ***H,*** [38] in a similar way that polarization, ***P***, is related to electric field, ***E***.

$$\boldsymbol{M} = \chi_m \boldsymbol{H} \tag{3}$$

Combining Eq. 2 and Eq. 3 gives a popular relation

$$\boldsymbol{B} = \mu_o(1 + \chi_m)\boldsymbol{H} = \mu_o\mu_r \boldsymbol{H} = \mu \boldsymbol{H} \tag{4}$$

where μ_r is the *relative permeability* of the media [39].
$\boldsymbol{M_s}$ is saturation magnetization, which is an important property for materials researchers to evaluate any magnet.
$\boldsymbol{M_r}$ is remanence magnetization which is the magnetization when $\boldsymbol{H} = 0$.
$\boldsymbol{B_r}$ is the remanence magnetic flux density, ***B***, when $\boldsymbol{H} = 0$, so $\boldsymbol{Br} = \mu_o \boldsymbol{M_r}$

The following text will provide the reader with a brief idea regarding the role of various alloying elements used in this research effort and its effect on H_c and B_r [33].

Cobalt: It is a γ stabilizer. A solutionization anneal is needed to homogenize it to a single α phase. Cobalt increases coercivity and Curie temperature.

Nickel: It is also a γ stabilizer. Hence, solutionization anneal temperature needs to be increased in order to homogenize it to a single α phase. Nickel increases Hc (less than Cobalt) while decreases Br.

Aluminum: It is an α stabilizer. It will be helpful in reducing the solutionization anneal temperature. Aluminum is expected to affect Hc positively.

Copper: It is an α stabilizer. Research shows that Copper affects Hc and Br positively and increases it. In AlNiCo 8 and AlNiCo 9 alloys, Cu precipitates out of the α2 phases into particles and is responsible for the magnetic separation between α1 and α2 phases. An increase in these phase separation leads to an increase in Hc.

Titanium: It is an α stabilizer and one of the most reactive elements. It reacts with impurities such as C, S, and N and purifies the magnet by forming precipitates with these elements. It helps in grain refining but it is detrimental for columnar grain growth. S and Te additions can help in regaining grain growth capabilities. Majority of grains are aligned perpendicular to the chill plate due to columnar grain growth and large shape anisotropy can be achieved if spinodal decomposition occurs in this direction. Titanium increases Hc at the expense of Br [40].

Niobium: It is an α stabilizer. It forms precipitate with Carbon. Carbon is a strong γ stabilizer and needs to be eliminated. Like Ti, Nb also inhibits columnar grain growth. Nb increases Hc, at the expense of Br [41].

Hafnium: It is used for enhancing high-temperature properties. It precipitates at the grain boundary and helps in improving creep properties. Recent studies related to Co-Hf magnets [7], motivated us to use Hf in this work.

A multi-dimensional random number generation algorithm [42] was used to distribute chemical concentrations of each of the alloying elements in the candidate alloys as uniformly as possible while maintaining the prescribed bounds on the minimum and maximum allowable values for the concentration of each of the alloying elements. The generated candidate alloy compositions were then examined for phase equilibria and associated magnetic properties using a thermodynamic database in the desired temperature range. These initial candidate alloys were manufactured, synthesized and tested for desired properties. Then, the experimentally obtained values of the properties were fitted with a multi-dimensional response surface. The desired properties were treated as objectives and were extremized simultaneously by utilizing a multi-objective optimization algorithm that optimized the concentrations of each of the alloying elements. This task was also performed by another conceptually different response surface and optimization algorithm for double-checking the results. A few of the best predicted Pareto optimal alloy compositions were then manufactured, synthesized and tested to evaluate their macroscopic properties. Several of these Pareto optimized alloys outperformed most of the candidate alloys on most of the objectives. This proves the efficacy of the combined meta-modeling and experimental

In this alloy design optimization methodology, the user must specify the minimum and maximum expected concentrations of a finite number of the most important alloying elements. For example, if the number of such elements in an alloy is 8 (e.g., Fe, Co, Ni, Al, Ti, Hf, Cu, Nb) and the number of simultaneous objectives is 3 (e.g., maximize magnetic energy density $(BH)_{max}$, magnetic remanence (Br) and magnetic intrinsic coercivity (H_c)), from experience with design optimization of Ni-base superalloys [16,18] and bulk metallic glasses [19-21] it is expected that an initial database of concentrations of approximately 80 alloys will need to be developed by utilizing Sobol's algorithm [42] to semi-randomly distribute the chemical concentrations of these alloys. The use of Sobol's algorithm is very helpful in distributing the initial concentrations in the best possible way so that the consequent multi-dimensional response surface fitting will be maximally accurate with the minimum number of available experimentally evaluated alloys. These 80 initial alloys must then be manufactured by casting them in an identical manner, thus avoiding variability in the manufacturing process. These casts should then be experimentally tested for the specified number of macroscopic properties (simultaneous objectives).

This information is then used for building approximation functions (multi-dimensional response surfaces) [43], which will further be enriched by the optimization code using modified radial basis functions and multiple artificial neural networks. These approximation functions are then optimized using a multi-objective evolutionary optimization algorithm. In this work, three multi-objective optimization algorithms were used: modeFrontier [44], IOSO [45] and MOHO [43]. At each optimization iteration, a multi-criterion optimization task with a specified number of Pareto front optimal points (for example, 10) needs to be solved. The results of this complex numerical optimization process will be chemical concentrations of the alloying elements in these 20 new alloys which the optimization algorithm predicted as belonging to the non-dominated Pareto optimal front, while accounting for a specified level of uncertainty of alloy casting and testing. Since the multi-dimensional response surfaces are fitted using a large number of points created by the artificial neural networks and the radial basis functions instead of exclusively experimental data, the initial accuracy of the fit of the response surface will be relatively low. Consequently, it could be expected that not all of the 10 new optimized alloys are actually superior to all of the

initial 80 alloys. To clarify this point, these 10 optimized alloys then need to be manufactured and experimentally evaluated for the multiple properties. This concludes the first design iteration. The second iteration starts by using all (80 + 10 = 90) experimentally evaluated alloys. The response surface building, enrichment, and optimization process is then repeated using these 90 data points with the same multiple objectives. Again, say, 10 new Pareto-optimal alloys are found by searching these improved response surfaces. These 10 newly Pareto-optimized alloys then need to be manufactured and experimentally tested to confirm that most of them are better than any of the 90 alloys used in the second iteration of the design optimization process. The third iteration then starts with all accumulated experimentally tested alloys (80 + 10 + 10 = 100), repeats all optimization steps, and results in a new set of optimized alloys. The entire iterative process continues typically 5-10 cycles until the Pareto front sufficiently converges.

A sensitivity analysis of each of the alloying elements was also performed to determine which of the alloying elements contributes the least to the desired macroscopic properties of the alloy. These elements can then be replaced with other candidate alloying elements such as not-so-rare earth elements.

Summary of Multi-Objective Optimization Concepts and Metamodels

The *multi*-objective optimization extremizes simultaneously a vector of n objective functions

$$F_i(\overline{x}) \qquad \text{for } i = 1, \ldots n \tag{5}$$

subject to a vector of m inequality constraints

$$g_j(\overline{x}) \leq 0 \qquad \text{for } j = 1, \ldots m \tag{6}$$

and a vector of k equality constraints

$$h_q(\overline{x}) = 0 \qquad \text{for } q = 1, \ldots k \tag{7}$$

where $\overline{x}$ is a vector of design variables that need to be optimized so that a vector of objective functions is simultaneously extremized.

In general, the solution of this problem is not unique, since each objective would like to attain its own extremum. With the introduction of the Pareto dominance concept [46] the possible solutions are divided in two subgroups: the *dominated* and the *non-dominated*. The solutions belonging to the second group are the "efficient" or the “best trade-off” solutions, that is, the ones for which it is not possible to improve any individual objective without deteriorating the values of at least some of the remaining objectives.

Metamodels and Multidimensional Design Spaces

In many optimization problems, evaluation of the objective function is extremely expensive and time-consuming. For example, optimizing chemical concentrations of each of the alloying elements in a multi-component alloy requires manufacturing each candidate alloy and evaluating its properties using classical experimental techniques. Even with the most efficient optimization algorithms, this means that often thousands of alloys having different chemical concentrations of

their constitutive elements would have to be manufactured and tested. This is understandably too expensive to be economically acceptable.

Therefore, for problems where objective function evaluations are already expensive and where the number of design variables is large and thus requires many such objective functions evaluations, the only economically viable approach to optimization is to use cheap and accurate surrogate models (metamodel) instead of the actual high-fidelity methods for evaluation of the objective functions. Such low-fidelity surrogate models are known as response surfaces [43,47] which, in case of more than three dimensions, become high-dimensional hypersurfaces that need to be fitted through the available, often small, original set of high-fidelity values of the objective function. Once the response surface (hypersurface) is created using an appropriate analytic formulation, it is very efficient to search such a hypersurface for its minima given a set of values of design variables supporting such a response surface.

One of the most popular mesh-free kernel approximation techniques is radial basis functions (RBFs). Initially, RBFs were developed for multivariate data and function interpolation. It was found that RBFs were able to construct an interpolation scheme with favorable properties such as high efficiency, good accuracy [47] and capability of dealing with scattered data, especially for higher-dimension problems. A convincing comparison [43] of a RFB-based-response surface method and several other popular methods demonstrated superiority of optimized RBF polynomial-based methods.

A Step-by-Step Iterative Design of Magnetic Alloys

We used a set of computational tools to develop a novel approach for design and optimization of high-temperature, high-intensity magnetic alloys. The steps involved in the proposed approach can be listed as follows:

1. Initial dataset: From our own expertise and the open literature, we defined the variable bounds of eight alloying elements that are to be used for the manufacture of magnets. One of the best-known quasi-random number generators, Sobol's algorithm [42], was used to generate chemical concentrations for an initial set of 80 candidate alloys. These alloys were screened on the basis of limited knowledge of phase equilibrium and magnetic properties from a commercial thermodynamic database, Factsage [48].

2. Manufacture and testing: These alloys were synthesized and tested for various properties of interest as shown in Table 3.

3. Response surface generation: This data was used to link alloy composition to desired properties by developing response surfaces for those specific properties. A commercial optimization package, modeFRONTIER [44] was used for this purpose. Response surfaces were tested on various accuracy measures and the most accurate one was chosen for further study. Various approaches [43] were used to develop response surfaces. These include Radial basis functions (RBF), Kriging, Anisotropic Kriging, and Evolutionary Design.

4. Multi-objective optimization: Response surfaces selected above were used to extremize the select macroscopic properties. It was observed that most of the optimization tasks yielded alloys with a similar chemical composition for a set of objectives. Hence, several optimization runs were performed to get a diverse pool of results. Various optimization

algorithms were used for this purpose. They include Non-dominated Sorting Genetic Algorithm II (NSGA2) [46], Multi-Objective Particle Swarm Optimization (MOPSO), Multi-Objective Simulated Annealing (MOSA) and FAST optimizer which uses response surface models (meta-models) to speed up the optimization process using search algorithms such as NSGA2, MOPSO, MOSA [44].

For the purpose of self-evaluation, this work was independently carried out at three different places using modified versions of these software packages:

a. Commercial optimization package, Indirect Optimization based on Self-Organization (IOSO) algorithm [45] was used because of its known robustness.

b. Hybrid response surface [43,47] was used because of its robustness, accuracy and computational efficiency. Multi-objective optimization was performed by Non-Dominated Sorting Genetic Algorithm (NSGA2) [46].

c. Surrogate model selection algorithm [43] was used because of its robustness and simplicity.

Pareto-optimized predictions from the above optimization packages were merged. From this set, we selected a few alloys for further manufacture and testing.

5. The work has been performed in cycles. Steps 2-5 were repeated until the improvements of multiple macroscopic properties of these magnetic alloys became negligible.

6. Sensitivity analysis: Various statistical tools were used to determine composition-property relations. This was done in order to find influential alloying elements for development of knowledge base. At the same time, the sensitivity analysis also helps in finding the least influential alloying elements that could be discarded to make way for introduction of affordable and readily available rare-earth elements.

This work will help in developing a knowledge base that will be useful to the research community in designing new alloys. In data-driven material science, knowledge discovery [9] for designing new materials requires:

a) Data: In this work, our database was a combination of experimentally verified data and Pareto-optimized predictions.

b) Correlations: Various linear and nonlinear correlation, clustering, and a principal component analysis tools were used to discover various trends in the dataset.

c) Theory: The above information can be coupled with theoretical knowledge to motivate the experimentalist to modifying standard manufacturer protocol for design of new alloys.

Summary of Experimental Work Performed by a Sub-Contractor (NCSU) Team

This project was to apply materials-by-design approach for magnetic materials without rare earths that iterates between computational optimization and experimental synthesis/property study, where computational multi-objective optimization drives experiments. AlNiCo alloys were chosen because of their low cost, acceptable permanent magnetic properties and especially the high temperature for applications (~400 ^{0}C).

Standardized procedures used during experimental work and testing performed at NCSU were:

Raw materials and weighing (All raw materials were from Alfa Aesar®)

Element	Symbol	Specification
Iron	Fe	Iron granules, 1-2 mm (0.04-0.08 in), 99.98% (metals basis)
Cobalt	Co	Cobalt pieces, 99.9+% (metals basis)
Aluminum	Al	Aluminum slug, 1.98 mm (0.078 in) dia x 8.0 mm (0.315 in) length, 99.99% (metals basis)
Nickel	Ni	Nickel slug, 3.175 mm (0.125in) dia x 3.175 mm (0.125in) length, 99.98% (metals basis) + 50 mmX50 mm, Nickel foil, 0.1 mm (0.004 in) thick, 99.5% (metals basis)
Titanium	Ti	Titanium granules, -15 mesh, 99.9% (metals basis excluding Na and K), 10g
Copper	Cu	Copper shot, 0.8-2 mm (0.03-0.08 in), 99.5% (metals basis), 100 g
Hafnium	Hf	Hafnium wire, 0.5 mm (0.02 in) dia, 99.95% (metals basis excluding Zr), Zr nominal 3%, 100 cm
Niobium	Nb	Niobium wire, 0.5 mm (0.02 in) dia, 99.96% (metals basis excluding Ta), 100 cm

According to the weight ratio of each element supplied by FIU, the mass of each element was calculated while the total mass for each sample was 5.1 gram. The reason for 5.1 grams was that the same mass was used to prepare ball-milling samples. Each alloying element was well stored and weighed out to within 0.001 grams in a glove box filled with high purity Argon (< 1 ppm oxygen). Each weighed sample was placed into glass vials within an Argon atmosphere.

Casting

Casting was performed with an arc melter. After weighing each of the eight elements, the sample was placed on copper hearth in the arc melter. The chamber of the arc melter was evacuated and refilled with argon three times to prevent oxidation. The chamber was refilled when the pressure reached 40 millitorr. After the third refill, the working pressure was set at 10 mmHg vacuum. The electric arc power was set to ~130 amps. If the sample was hard to melt after a few seconds, the power was increased to ~145 amps. With the power supply and water cooler on, the electric arc was started by making contact between the electrode tip and the tungsten pin. A small piece of titanium was melted first in order to react with any remaining oxygen.

During the initial arc melting, the goal was to melt the sample and form a single piece of alloy. After five to ten seconds of arc melting, the sample was left to cool for approximately two minutes. Then, it was safe to refill the pressure to 1 atm and open the arc melter. When a single piece of alloy was formed, the sample was flipped and the process of evacuating three times and melting was repeated two more times which includes flipping the sample after each time being melted.

After flipping and melting twice, the hearth is tilted to an angle of approximately 45 degrees and the sample is moved to the far right of the copper hearth where there is a notch that allows the sample to be cast. At this angle, when the sample is melted, it will pour into the copper mold and form a seven millimeter diameter cylinder. After casting, the samples were re-weighed to account for any alterations from the treatments.

Cutting

The sample alloy melts solidified before reaching the bottom of the mold, causing each end of the solidified alloy cylinder to be rounded. This section of the sample was cut off by a diamond tipped blade. From the remaining cylinder, a three millimeter thick disc was cut (Fig. 2). These cylindrical samples are weighed and placed into new glass vials marked with their respective mass.

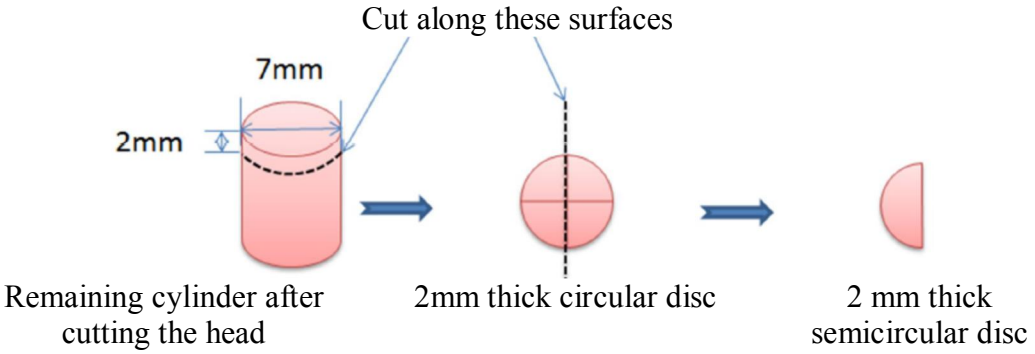

Fig. 2 Cutting the cast alloy rod

Solutionizing treatment

The solutionizing treatment was performed in a horizontal tube furnace. There was a 10 centimeter wide hot zone in the middle of the furnace. The samples were placed separately on Al_2O_3 plates and annealed for 30 minutes at 1250 ^{0}C in the hot zone with forming gas (98%Argon + 2%Hydrogen) flowing. After annealing for 30 minutes, the plate with samples was pulled out with a metal bar and quenched into cold water. The time from pull out to quench was less than 5 seconds. Samples were then dried and cleaned before weighing to distinguish them and placed back into corresponding vials.

Thermomagnetic treatment

Thermomagnetic treatment was performed in a vertical furnace in the center of a superconducting magnet (Fig.3). Three thermocouples (#1, #2, and #3) were used for monitoring temperature.

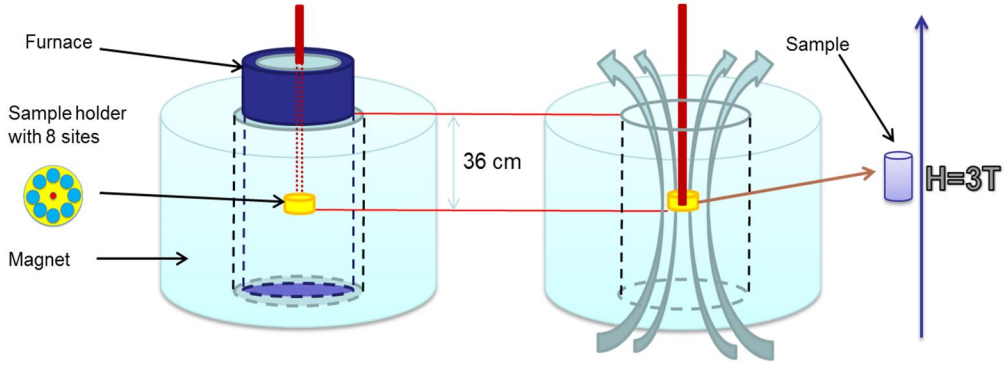

Fig.3 A schematic image of the facilities for the thermomagnetic treatment

Thermocouples #1 and #2 were fixed ~3 millimeter away from the samples, while #1 was used to gather data for the computer and #2 to control the furnace automatically to get the temperature we want; #3 was fixed between the metal shell and the ceramic core for the safety of the furnace.

The samples were fixed with their long axis aligned with the magnetic field in the center of the magnet (Fig.4). The uniform zone of magnetic field was 36 cm from upper surface of the magnet, so the samples were fixed in that zone. When the samples were installed well, thermomagnetic treatment was initiated and was divided into 6 steps as follows:

1) Ramp up the magnet to 3 T (2 hour)
2) Heat up the furnace to 800 ^{0}C (35 min)
3) Anneal the samples for 10 min at 800 ^{0}C in 3 T magnetic fields when the temperature is stable at 800 ^{0}C. (Total time is around 20 min, see Fig. 4)
4) Cool down the furnace to lower than 200 ^{0}C (around 4 hour)
5) Ramp down the magnet to 0 T (2 hour)
6) Remove the sample

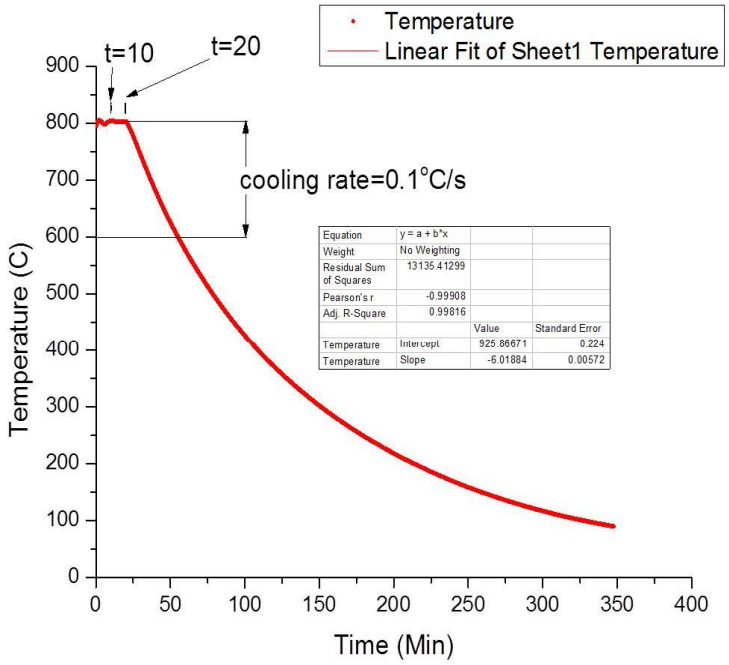

Fig.4 Temperature vs time during thermomagnetic treatment

5. SQUID test

The magnetic results are tested with SQUID. The sample was mounted with GE7031 varnish at the designated spot in the brass sample holder. After drying 90 min with a drying gun, sample holder was installed into the chamber of SQUID and the test was started. The changing process of the magnetic field was from zero Tesla to 3T then to -3T and then back to 3T again. We obtained a magnetic hysteresis loop from this in which x axis is the moment and y axis is the field strength.

6. Calculation

We could only obtain Hc (Oe), Mr (emu), Ms (emu) in CGS unit system from the loop, so we needed to calculate and convert all results into SI unit system.

Results of the Combined Computational-Experimental Iterative Design

Results of this mixed computational-experimental approach when designing and experimentally verifying candidate alloys, are presented in the next few figures and in Tables 1, 2 and 3 that provide details important to understand the numerical values used in this work.

Table 1: Quantities to be simultaneously extremized using multi-objective optimization

	Properties	Units	Objective
1	Magnetic energy density ($(BH)_{max}$)	kg m^{-1} s^{-2}	Maximize
2	Magnetic coercivity (H_c)	Oersted	Maximize
3	Magnetic remanence (B_r)	Tesla	Maximize
4	Saturation magnetization (M_s)	Emu/g	Maximize
5	Remanence magnetization (M_r)	Emu/g	Maximize
6	$(BH)_{max}$/mass	m^{-1} s^{-2}	Maximize
7	Magnetic permeability (μ)	kg m A^{-2} s^{-2}	Maximize
8	Cost of raw material (cost)	$/kg	Minimize
9	Intrinsic coercive field (jH_c)	A m^{-1}	Maximize
10	Density(ρ)	Kg m^{-3}	Minimize

Table 2: Concentration bounds used for optimization of AlNiCo type alloys

Alloys number	1-85	86-143	144-173
Alloying elements	Concentration bounds (wt. percent)		
Cobalt(Co)	24 - 40	24 - 38	22.8 - 39.9
Nickel (Ni)	13 - 15	13 - 15	12.35 - 15.75
Aluminum (Al)	7 - 9	7 - 12	6.65 - 12.6
Titanium (Ti)	0.1 - 8	4 - 11	3.8 - 11.55
Hafnium (Hf)	0.1 - 8	0.1 - 3	0.095 - 3.15
Copper (Cu)	0 - 6	0 - 3	0.4 - 5
Niobium (Nb)	0 - 2	0 - 1	0 - 1.5
Iron (Fe)	Balance to 100 percent		

Table 3: Design cycle and alloy number

Cycle number	Number of alloys designed	Best alloy in the cycle
1	1-80	#30
2	81-85	#84
3	86-90	#86
4	91-110	#95
5	111-120	#117
6	120-138	#124
7	139-143	#139
8	144-150	#150
9	150-160	#157
10	160-165	#162
11	166-173	#169

In this project, we have worked through 11 iterative cycles of design and optimization, each of them including its own experimental validation as follows.

1. Cycle 1 (Alloys 1-80): Initial alloy compositions were predicted by Sobol's algorithm [42] and the initial set of 80 elements was chosen for manufacture and testing. Thereafter, we proceeded further with design and optimization with the goal of improved results.

2. Cycle 2 (Alloys 81-85): One of the predicted alloys (alloy 84) outperformed the initial set of alloys as well as the other Pareto-optimized predictions. This demonstrates the efficacy of the current approach and we moved forward with the objective of further improvements. The variable bounds were updated. New bounds (for alloy 86-90) are listed in Table 3.

3. Cycle 3 (Alloys 86-90): Alloy 86 was the best candidate in this set. Measured properties of the new set (alloy 86-90) were in the vicinity of the previous pool of alloys. One of the reasons for this can be non-uniform distribution of alloying elements in the variable space. Since, there was no significant improvement; next set of alloys were predicted by Sobol's algorithm so as to provide additional support points in the variable space for development of response surfaces with improved accuracy.

4. Cycle 4 (Alloys 91-110): Alloy 95 was the best performer in this group. Our approach of providing more support points for the response surfaces proved helpful in the improvement of properties. Alloy 95 had an H_c of 980 Oe (against 750 Oe for the previous best alloy 84).

5. Cycle 5 (Alloys 111-120): Alloy 117 is the best alloy in this dataset in terms of ((BH)max). There was a significant improvement in the properties of the new alloys. Alloy 111 and 114 had an H_c of 1050 Oe while alloy 117 reported 1000 Oe (against 980 Oe for the previous best alloy 95).

6. Cycle 6 (Alloys 121-138): Alloy 124 was the best performer in this group. There was a significant improvement in both $((BH)_{max})$ and H_c.

7. Cycle 7 (Alloys 139-143): Alloy 139 was the best performer in this group. Its properties were in the vicinity of alloy 124. Since, there was no significant improvement in the desired properties; we halted the design and optimization process to perform a sensitivity analysis of the variables and associated properties.

Cycles 8-11 (Alloys 144-173): In these cycles, variable bounds were relaxed by 5 percent while the methodology remained the same.

8. Cycle 8 (Alloys 144-150): Alloys predicted by modeFRONTIER. Marginal improvement in H_c was observed, but there was no significant improvement in other properties.

9. Cycle 9 (Alloys 151-160): Alloys predicted by Surrogate Model (SM) selection algorithm. There was no significant improvement in any of the properties.

10. Cycle 10 (Alloys 161-165): Alloys predicted by modeFRONTIER. Marginal improvement in H_c. However, no significant improvement in other properties.

11. Cycle 11 (Alloys 166-173): Alloys predicted by Hybrid response surface and modeFRONTIER. Marginal improvement in H_c was observed, but there was still no significant improvement in other properties.

This project had two main periods. For the first period (2013-2014), Florida International University (FIU) supplied an initial database of 80 alloys and NCSU synthesized & characterized these initial 80 alloys and reported the magnetic properties to FIU for composition optimization. For the second period (2014-2015), FIU used these results and subsequent results to identify 100 new alloy compositions, which were synthesized & characterized by NCSU. All of 180 alloys (compositions are in the Appendix A) were produced with the standardized procedures.

Using FIU's multi-objective optimization and statistical tools, the new stoichiometries were identified with high H_c and $(BH)_{max}$. During the first period, max H_c = 600 Oe and max $(BH)_{max}$ = 0.5 MGOe, while the second period (using standardized processing only) max H_c = 1100 – 1180 Oe (5 different compositions) and max $(BH)_{max}$ = 1.5 MGOe, demonstrating that this iterative combined experimental/computational alloy design approach is effective.

Figures 5, 6 and 7 show the comparison between various approaches for a set of properties. Note that (x) symbols were experimental results for the initial 80 alloys having their concentrations of alloying elements obtained by using a quasi-random sequence generator [42]. Diamond symbols show experimental results for the set of Pareto-optimized alloys predicted by the IOSO optimizer based on a response surface created with the initial random 80 alloys.

It can be observed that the alloys predicted by meta-modeling and optimization dominate the ones predicted by Sobol's algorithm [42]. One can observe significant improvement over the cycles. Experimentally verified H_c values are at comparable to those in commercial AlNiCo alloys [8]. We expect improvement in $(BH)_{max}$ and B_r values in the next few cycles. At this point, we have a significant amount of experimentally verified data. Hence, we felt the need to perform a sensitivity analysis of the response surfaces and look for patterns in the dataset.

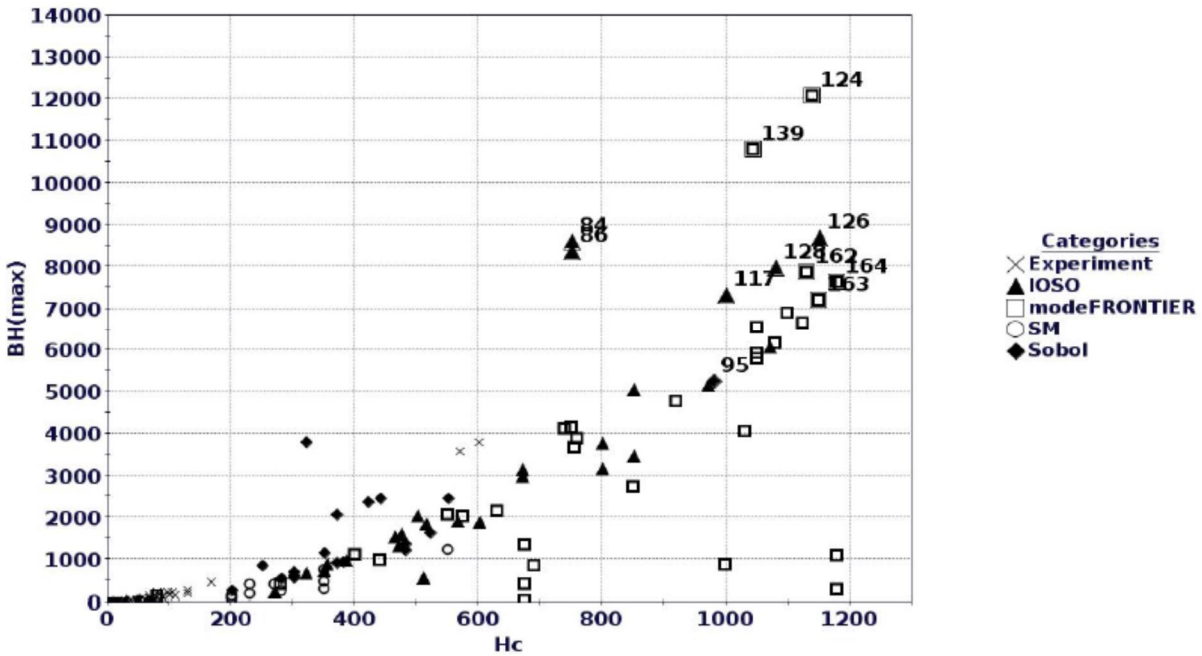

Fig. 5 Magnetic energy density (BH)max *vs.* magnetic coercivity (Hc); comparison of solutions by various approaches

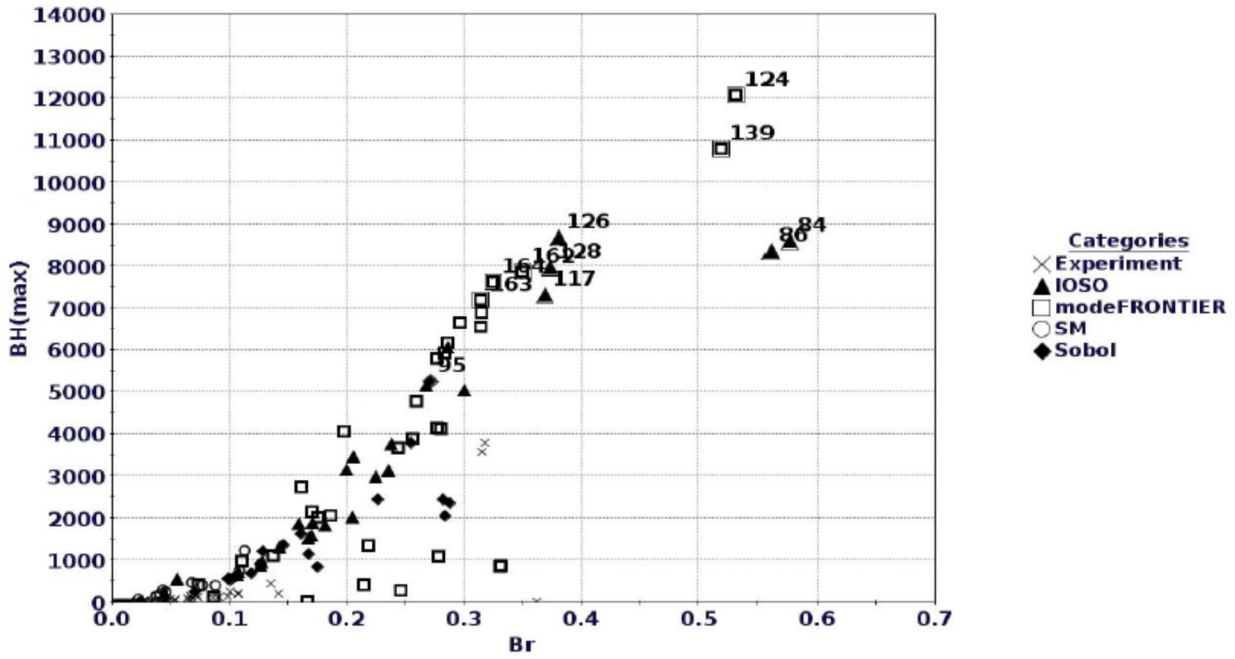

Fig. 6 Magnetic energy density (BH)max *vs.* magnetic remanence (Br): comparison of solutions by various approaches

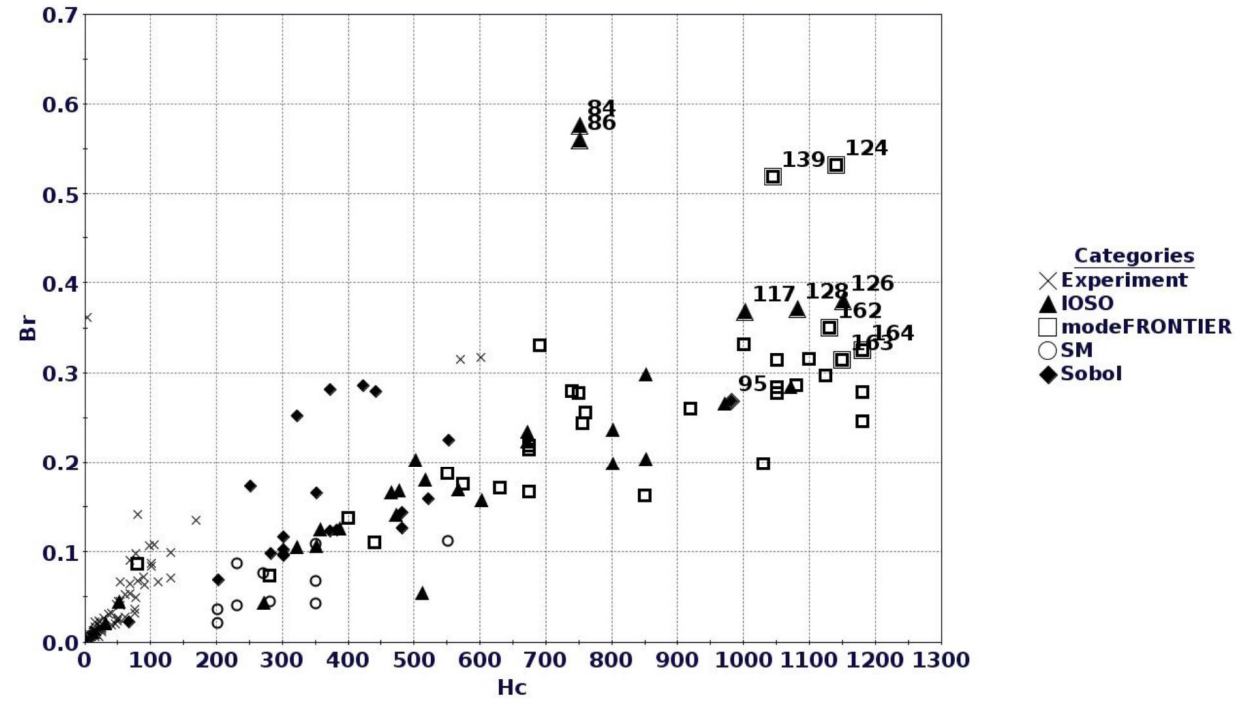

Fig. 7 Magnetic remanence (Br) *vs.* magnetic coercivity (Hc): comparison of solutions by various approaches.

The magnetic properties are driven by microstructure shape anisotropy and spinodal decomposition that forms a fine modulated microstructure on nano-scale, which varies from alloy

to alloy. Typical samples were characterized by NCSU from micro-scale to nano-scale and finally to atomic scale. Some important characterizing results are shown below.

Scanning electron microscope (SEM) images in Fig.8 show the clear difference in morphology and white phase between center and outer areas. Table 4 is the energy-dispersive X-ray spectroscopy (EDS) results of distribution of elements in these areas with different contrast in AlNiCo alloy. The "white" areas are Fe-deficient and Hf and Nb rich so Hf and Nb diffuse to the center area during the thermomagnetic treatment in micro-scale.

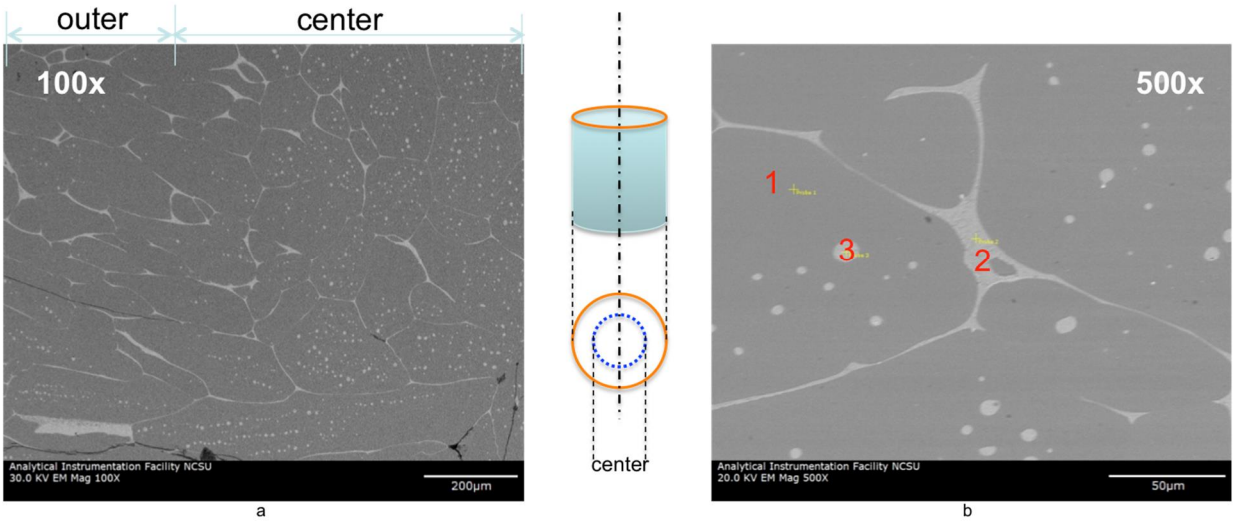

Fig.8 Scanning electron microscope (SEM) images viewing along the transverse orientation (// the magnetic field): (a) 100x, (b) 500x.

Table 4: Energy-dispersive X-ray spectroscopy (EDS) of distribution of elements in the areas with different contrast

Name	Fe	Co	Ni	Al	Ti	Hf	Cu	Nb	C	O
Targeted composition	32.35	36.85	13.54	7.2	4.11	2.06	2.93	0.93	0	0
Sample "net" (Fig.1 (a))	32.09	35.64	11.99	8.76	5.21	0.04	2.56	1.32	1.54	0.86
Point 1(Fig.1 (b))	32.5	35.45	14.32	9.67	4.3	0	3.32	0.44	0	0
Point 2(Fig.1 (b))	23.88	34.79	14.99	6.85	4.78	7.95	3.77	2.96	0.03	0
Point 3(Fig.1 (b))	25.78	34.49	14.43	8.88	4.92	5.89	3.42	2.17	0.03	0

Figure 9 is transmission electron microscopy (TEM) images along transverse (parallel to the magnetic field) and longitudinal (perpendicular to the magnetic field) orientations. Along the [001] direction, the feature of AlNiCo is observed: α_1 phases (light square, hard magnetic phase, mainly Fe and Co), α_2 phases (dark matrix, soft magnetic phase, mainly Ni and Al) and Cu bridges (red arrow); along the [010] direction, needle like α_1 is observed.

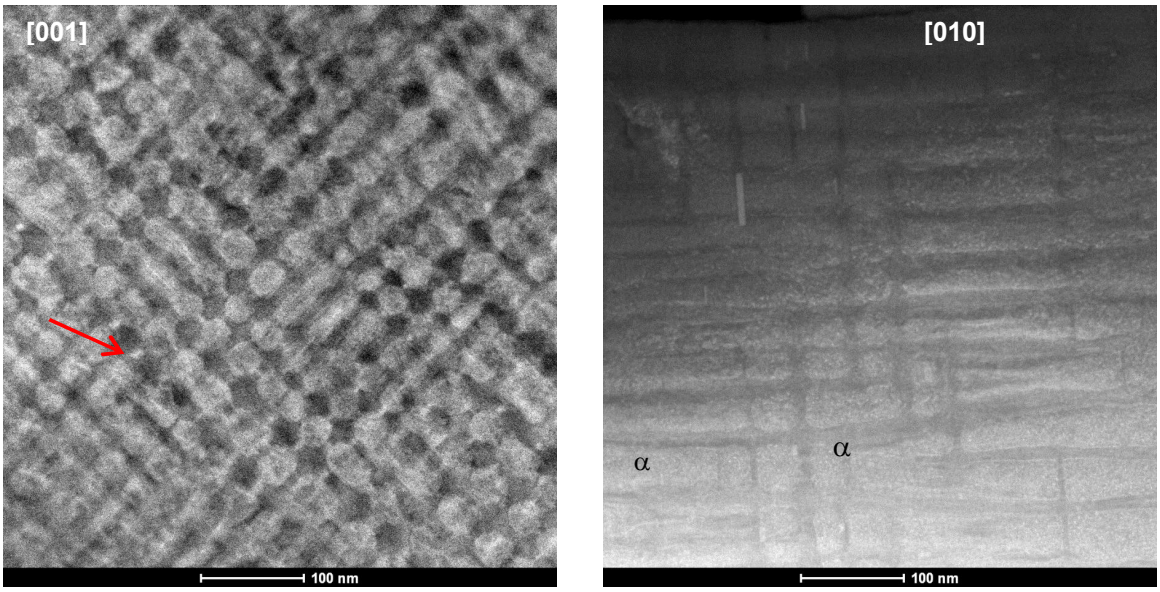

Fig. 9 Transmission Electron Microscopy (TEM) images along (a) transverse (parallel to the magnetic field) and (b) longitudinal (perpendicular to the magnetic field) orientations

Figure 10 is the atomic scale characterization that high-resolution high angle annular dark field (HAADF) images in [001], [011] and [111] directions. The structure of α_2 in this alloy should be $L2_1$. The position of Al and (Fe, Ti) atoms are set on either the (0, 0, 0) or (1⁄2, 0, 0) sites, respectively; Al has a relatively small atomic number, so in the [001] direction, the dark (Al atoms) and light (Fe or Ti atoms) spots are alternately observed. In the [011], the rows only fill with Al atoms will become unclear in the column of Al, Fe and Ni. In the [111], no obvious difference of contrast is observed because Al only occupies ¼ sites.

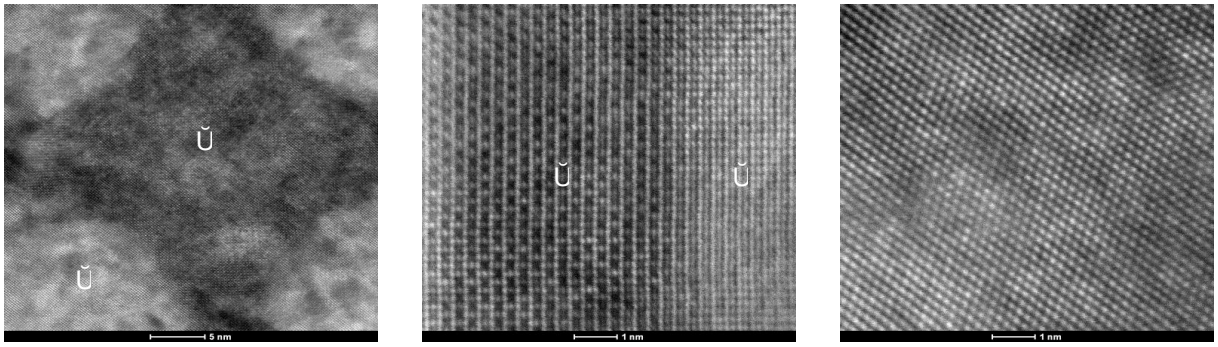

Fig.10 High-resolution high Angle Annular Dark Field (HAADF) images of (a) α_1 (light corner) and α_2 (dark center) in [001]; (b) α_1 (light right) and α_2 (dark left) in [011]; (c) α_1 or α_2 in [111].

Some good results were obtained with thorough research on the Cu-rich bridges of the AlNiCo alloys after the thermomagnetic treatment. A manuscript will be submitted soon to a journal. These results are important to develop the fundamental understanding of spinodal decomposition and structure-composition-magnetic behavior relationships in AlNiCo alloys.

Results of Statistical Methods Used to Find Trends and Chemistry-Properties Relations

This was done in order to determine the composition-property relationship. Another purpose was to find various trends and patterns within the dataset. Initially, Pearson's linear correlation method was used, which is applicable to linear problems only. It was followed by various approaches to determining non-linear trends within a dataset [31].

Single Variable Response (SVR)

This is a methodology that is often applied for qualitative analysis of the training results obtained from Evolutionary Neural Network [49] and Bi-Objective Genetic Programming [50,26]. In SVR, a trend is created by generating values between zero and one on a time scale. The trend line is irregular. Specifically, there are regions of constant values, sharp increases, and sharp decreases in the line. This has been referred to as an input signal in the following text. For SVR testing, the input signal (a trend of variation) was used for one of the variables while the other variables were kept constant at an average value. The various responses were tabulated in Table 5 for each of the models. For the responses, the following terminologies were used:

Dir: This means that the model output increases by increasing the value of an input signal and decreases by decreasing the input value.

Inv: This means that a particular variable increase will cause the property value to decrease and *vice versa*.

Nil: This means that the model was unable to find any correlation between that particular variable and the model output.

Mix: This means that the model has a different response for a different set of data of any particular variable.

Since, the dataset is quite noisy, the responses were mixed (Table 5). However, a few important findings can be listed as follows:

1) Copper shows a direct response for H_c and B_r. Thus, response surface predictions are of comparable accuracy with available results in the open literature.
2) Hafnium shows a direct response for $H_c$and B_r. Further experiments/ data analysis are needed before reaching a conclusion regarding the effect of Hf on H_c and B_r as it has not been previously used in AlNiCo alloys.
3) Nickel shows response for $(BH)_{max}$.

These findings are promising as they mimic the findings from the literature. Hence, meta-modeling can prove to be an asset for developing alloys in the future. In order to proceed further, we need to evaluate our findings by other data-mining techniques.

Table 5: Single variable response (SVR) for various macroscopic properties of AlNiCo type alloys

Objective No.	Properties	Variable response							
		Fe	Co	Ni	Al	Ti	Hf	Cu	Nb
1	Magnetic energy density ((BH)max)	Nil	Nil	Mix	Nil	Nil	Nil	Nil	Nil
2	Magnetic coercivity (Hc)	Mix	Mix	Mix	Inv	Mix	Dir	Dir	Mix
3	Magnetic remanence (Br)	Mix	Mix	Mix	Inv	Mix	Dir	Dir	Inv
4	Saturation magnetization (Ms)	Dir	Inv	Dir	Mix	Inv	Dir	Mix	Mix

5	Remanence magnetization (Mr)	Nil	Nil	Nil	Nil	Nil	Nil	Nil	Nil
6	(BH)max/mass	Nil	Nil	Nil	Nil	Nil	Nil	Nil	Nil
7	Magnetic permeability (μ)	Mix	Mix	Mix	Mix	Inv	Mix	Mix	Mix
8	Cost of raw material (cost)	Inv	Inv	Inv	Dir	Dir	Dir	Inv	Dir
9	Intrinsic coercive field (jHc)	Mix	Mix	Mix	Inv	Inv	Mix	Dir	Mix
10	Density(ρ)	Mix	Dir	Mix	Inv	Inv	Mix	Mix	Dir

Principal Component Analysis (PCA)

Principal component analysis can be classified as an unsupervised machine-learning algorithm [31,32]. It was performed in order to determine correlations between variables and various properties by reducing the dimensionality of the dataset without losing much information. PCA uses an orthogonal transformation to convert a set of usually correlated variables (or properties) into a set of values of linearly uncorrelated variables known as Principal Components (PCs). Hence, each PC is a linear combination of all the original descriptors (variables and properties). The first principal component (PC1) accounts for maximum variance in the dataset, followed by PC2 and so on [9,44]. Thus, it is possible to visualize a high dimensional dataset by choosing first two or three principal components [31,32]. It is also used for identifying patterns in data, as patterns may be hard to find in high-dimensional data sets.

PCA analysis was conducted separately for design variables (alloying elements) and targeted properties. For design variables, all the eight elements were included for PCA analysis. We have 8 design variables, thus there will be maximum of 8 PCs.

For targeted properties, it can be observed that apart from $(BH)_{max}$/mass, all other properties were measured independently. $(BH)_{max}$/mass was thus removed from further analysis to reduce complexity of the problem. We are left with 9 targeted properties, thus, there will be a maximum of 9 principal components. Prior to PCA analysis, three important terms need to be discussed for better understanding of the analysis results:

a) Scree plot: It is a plot between Eigen values and component number. It is an important parameter used to select the number of components required to represent the complete dataset. Usually, components with eigenvalues above one (1) are chosen for further analysis. It can be seen from the figures in the later part that the scree plot usually flattens below eigenvalue 1. This means that the later components do not have any significant effect on the dataset. Since each successive component accounts for comparatively less variance, the least influential components can be ignored from further analysis.

b) Eigenvalues: are the variances of the principal components. Principal components analysis was conducted on the correlation matrix. Here, the variables were standardized, so that each variable has a variance of one, and the total variance is equal to the number of variables used in the analysis. Thus, there will be eight PC for elements and nine PC for properties. The first component will always account for the most variance (and hence will have the highest eigenvalue). Next, components will account for as much of the left over

variance as they can. Hence, each successive component will account for comparatively less variance (hence less eigenvalues) than the one preceding it.

c) Component plot: After the required number of components are chosen, these components are plotted against each other, while the original variables (or properties) are plotted on this reduced space. Orientation of a certain variable (or property) on the reduced space determines its contribution towards a certain PC. That is, if the variable is positioned along PC1 on the 0-line perpendicular to PC2, this variable will have maximum influence on PC1 and minimum influence on PC2. This will be better explained with the corresponding figures in the latter part of the text.

In the component plot, the alloys are clustered by K-means clustering method to classify the alloys into different clusters. Alloys that belong to the same cluster have the same symbol. A few of the best alloys mentioned in Table 5 are plotted in these figures. In these figures, variables (elements) are plotted as arrows. Arrows represent the relative contribution of the original variables to the variability along the PCs. In these figures, the longer the arrows, the stronger are their contributions. Additionally, an arrow orthogonal to a certain PC has null effect on that PC, while an arrow that is collinear to a certain PC contributes only to that certain PC.

We classified the dataset into four sets and performed the PC analysis on individual sets in order to extract information from one set and then cross-check it with the findings of other sets. In all of these cases, PC1, PC2, and PC3 were able to capture most of the variance of the dataset. Dataset was classified as follows:

a) Experimental: Alloys #1-80

b) Optimization: Alloys # 81-173

c) Data categorized based on Multi-Criterion Decision Making (MCDM): 40 alloys were selected.

d) Whole dataset: Alloys # 1-173.

We used a popular statistical software, IBM SPSS [51], and Multivariate Data Analysis (MVA) node in optimization package modeFRONTIER [44] for this work.

a) Experimental: Alloys 1-80

These 80 alloys represent the initial set of compositions predicted by Sobol's semi-random sequence generation algorithm [42]. Hence, we did not perform PCA on the elements. Various properties were analyzed and reported below. Scree plots were created in order to determine the number of effective principal components required to represent the whole dataset. It was found that two PCs are able to extract most of the information from the dataset. Figure 13 shows the scree plot for the properties, while Figure 14 shows the orientation of various properties in the PC space.

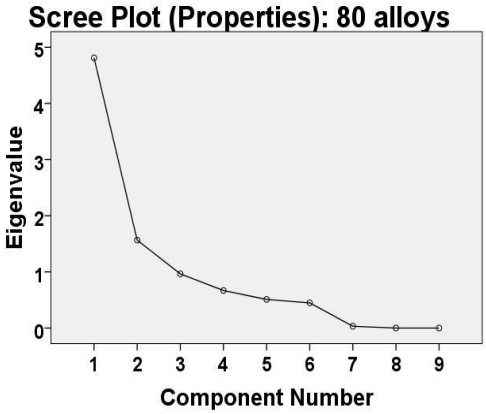

Fig. 11 Scree plot for PC analysis: Two PC components were chosen

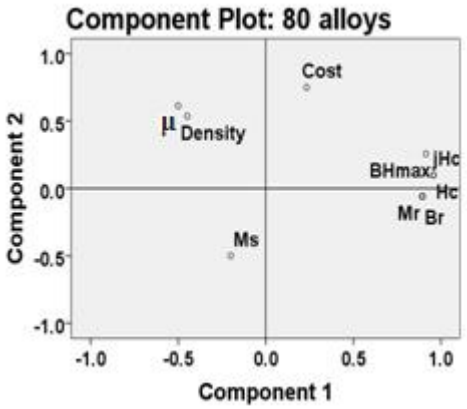

Fig. 12 Orientation of various properties in the PCA space

Figure 12 shows that $(BH)_{max}$, jH_c, H_c, M_r and B_r have maximum effect on PC1 while cost and M_s has maximum effect on PC2. Density and μ have similar effects on both PC. It can be seen that H_c and jH_c coincide at the same spot thus H_c and jH_c seems to be dependent on each other. It makes sense, as one is the inverse of the other. Similarly, M_r and B_r can be clustered together and μ and density can be taken as another cluster. This means that properties that form a cluster may affect, or may be dependent on, each other. Analysis of other datasets will further clarify these findings.

b) Optimization: Alloys 81-173

In this data, we went for PC analysis for the elements. From scree plot in Figure 13, it was found that three PCs are able to extract most of the information from the dataset. Figure 13 shows the scree plot for the elements while Figure 14 shows the position of various elements in the PC space.

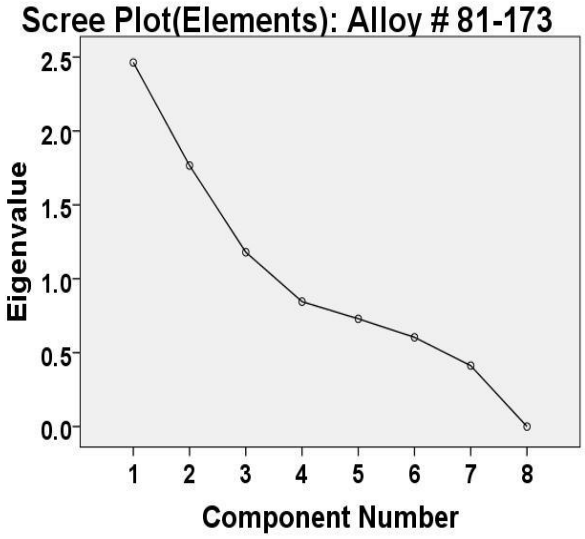

Figure 13 Scree plot for PC analysis: Three PC components were chosen

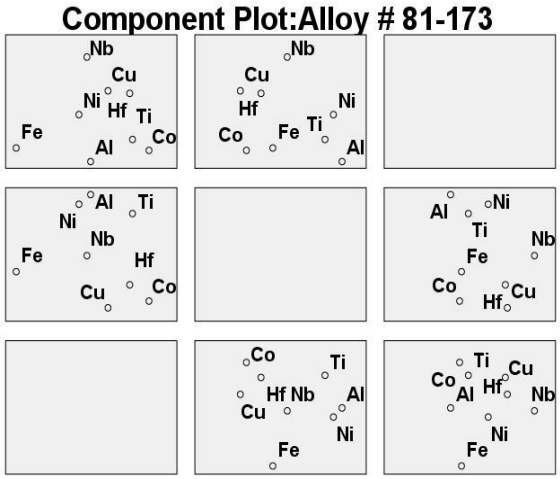

Figure 14 Orientation of various elements in the PC space

In Fig. 14, one can observe that elements have mixed effect on the three selected PCs. Since various optimizers and Sobol's algorithm have predicted these alloys composition, it seems to be properly distributed in the variable space. Hence, such a relation can be expected.

Upon close observation, it can be seen that Cu and Hf are close enough to form a cluster. This means that Cu and Hf may affect the properties of the alloy in a similar way. From SVR analysis, both Cu and Hf showed a direct response for H_c and B_r. Hf usually precipitates at the grain boundaries and enhances high temperature properties. However, it has been rarely used in AlNiCo alloys; hence, this finding can be helpful for the experimentalist to proceed forward for Hf addition in AlNiCo alloys. This must be analyzed further in other datasets before moving for microstructure analysis. Ni and Al can also be clustered together and seems to have similar effect. This can be supported from the literature, as there exists Ni-Al rich phase in these alloys.

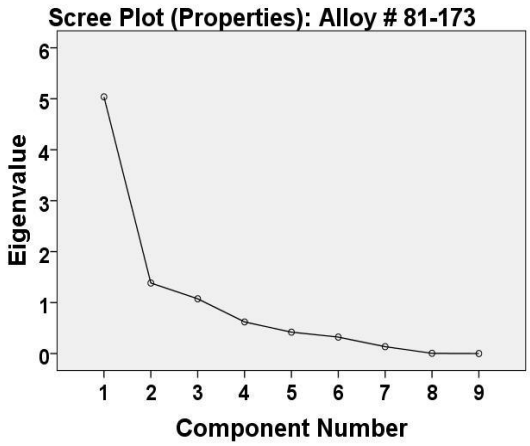

Fig. 15 Scree plot for PC analysis: Three PC components were chosen

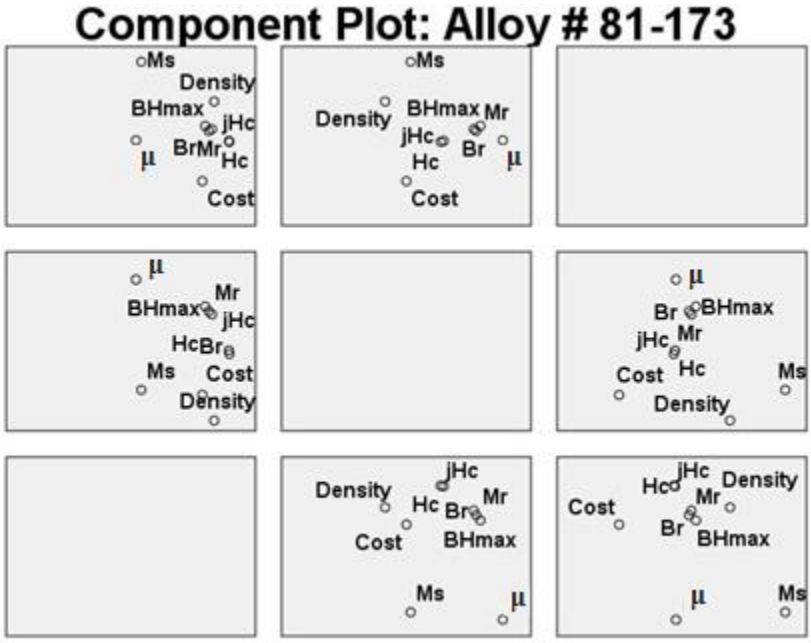

Fig. 16 Orientation of various properties in the PC space

It was found that three PCs are able to extract most of the information from the dataset. Figure 15 shows the scree plot for the elements, while Figure 16 shows the position of various properties in the PC space. In Fig.16, H_c and jH_c are clustered together. It can be seen that B_r, M_r, and $(BH)_{max}$ can be clustered as well. B_r and M_r were clustered in the previous analysis. Hence, these properties may be correlated (or dependent) on each other.

c) Data categorized based on Multi-Criterion Decision Making (MCDM): 40 alloys were selected. Due to software limitations, we focused on optimizing $(BH)_{max}$, H_c and B_r only. We left the other properties of interest though they are quite important for the magnet. In this part, we selected 40 alloys based on objectives defined in Table 1. We used MCDM methodology to select these alloys.

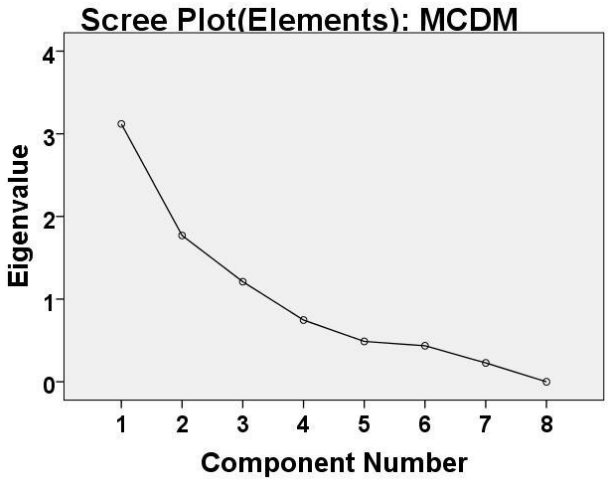

Fig. 17 Scree plot for PC analysis: Three PC components were chosen

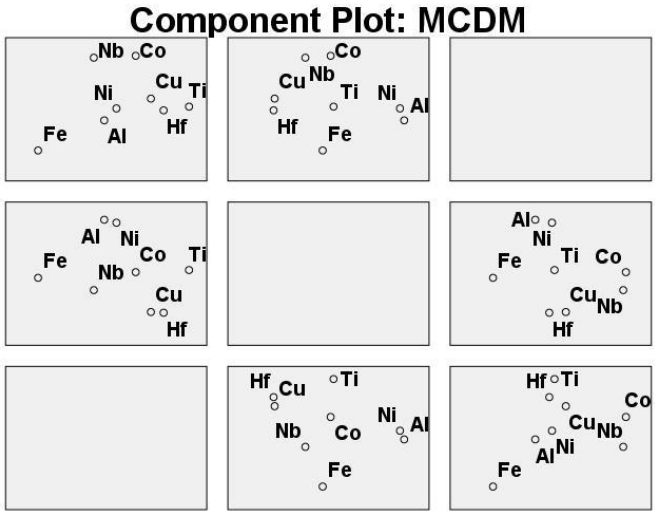

Fig. 18 Orientation of various elements in the PC space

Based on eigenvalues, three PCs were chosen (Figure 17). Figure 18 shows the orientation of various elements on the PC space. Figure 18 supports our finding from the previous set regarding

Copper and Hafnium. In this set too, Cu and Hf can be clustered together. Similarly, Ni and Al can be clustered together.

Figure 19 shows scree plot for various properties, while Figure 20 shows the orientation of these properties in the PC space. In Fig. 20, Mr and Br can be clustered and hence these properties may be dependent on each other. $(BH)_{max}$ does not seem to be part of the cluster anymore, but is close to it. Finally, we can proceed towards analyzing the whole dataset.

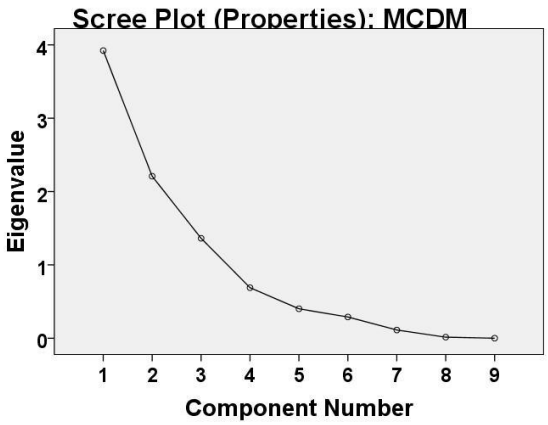

Fig. 19 Scree plot for PC analysis: Three PC components were chosen

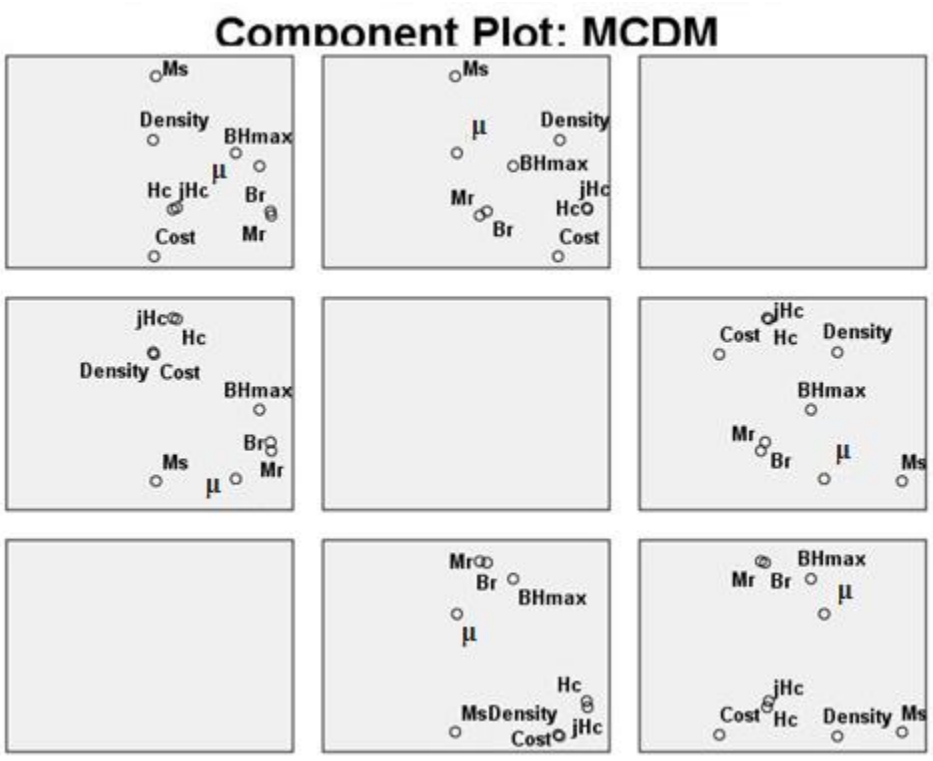

Fig. 20 Orientation of various properties in the PC space

c) Whole dataset: Alloys 1-173.

Here, the complete dataset was used for analysis. Figure 21 shows the plot for various elements. Based on eigenvalues, three PCs are able to extract most of the information from the dataset.

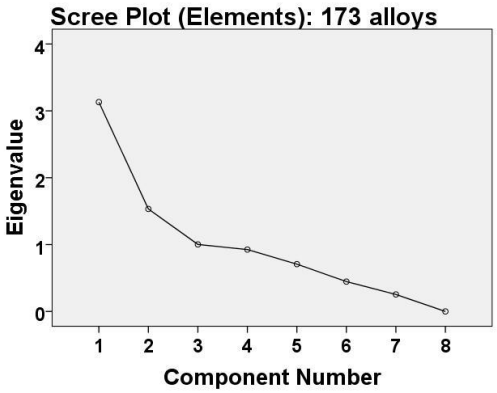

Fig. 21 Scree plot for PC analysis: Three PC components were chosen

Figure 22 shows the orientation of various elements in the PC space. Cu and Hf can be clustered together (Fig. 22). In PC1 *vs.* PC2 (top corner), Ti can also be clustered along with Cu and Hf. Ni and Al can be clustered together. Hence, we have sufficient information from the above analysis to move forward towards microstructure analysis.

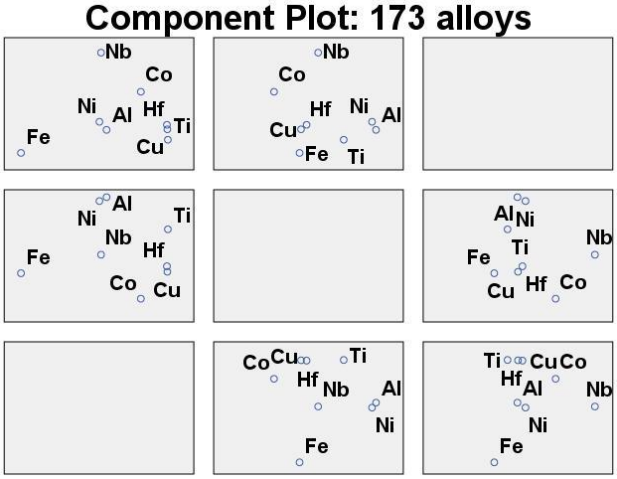

Fig. 22 Orientation of various elements in the PC space

Figure 23 shows the scree plot for various properties. Based on eigenvalues, two PC's can extract most of the information from the dataset. Figure 24 shows the orientation of various elements in the PC space. In Fig.24, it can be observed that $(BH)_{max}$, B_r, μ, H_c, jH_c and M_r contributes strongly on PC1, while Ms and density strongly contributes towards PC2. $(BH)_{max}$, B_r, and M_r can be clustered together. These findings are in line with the previous observations.

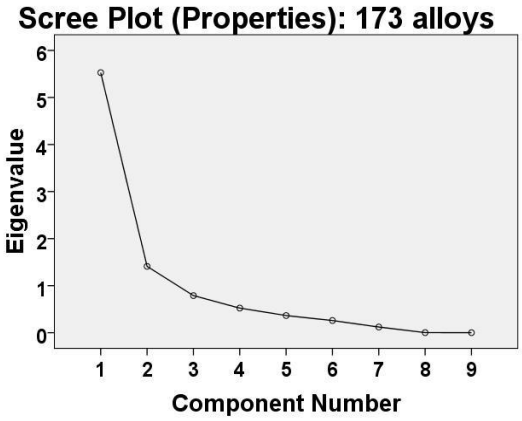

Fig. 23 Scree plot for PC analysis: Two PC components were chosen

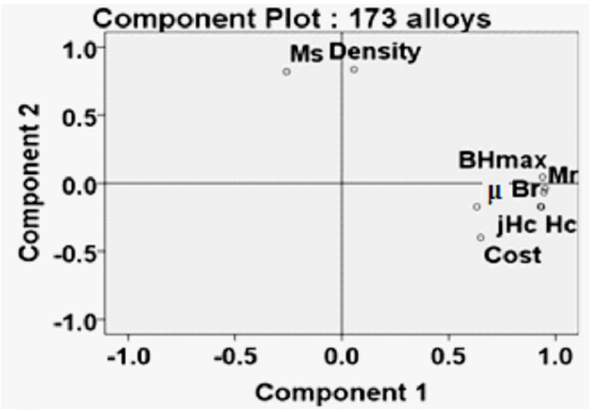

Fig. 24 Orientation of various properties in the PC space

Hence, we can proceed further and look towards the orientation of various alloys on the PC space along with the alloying elements. Here, the alloys were plotted on the PC space along with the elements. Here, the element's contribution towards a certain PC is related to the length and orientation of the arrow corresponding to that particular PC. Cluster analysis was performed by K-means clustering (Kaufman approach). Davies-Bouldin index (D-B index), is a measure of quality of clustering and it is used for determining the appropriate number of clusters into which the dataset can be divided. D-B index is the sum ratio of internal variance of each cluster with inter-cluster distance. In partitive clustering, one prefers small internal variance of each cluster along with high inter-cluster distances. Thus, D-B- index needs to be minimized. That is, number of clusters corresponding to lowest D-B index is applied on the dataset. Based on D-B index, the data set was divided into 8 clusters. Alloys belonging to different clusters were denoted by different symbols in Fig. 25 which used 173 alloys that were actually manufactured and experimentally evaluated. A few alloys were marked in order to avoid overlapping and give clear understanding. These alloys are from the best alloys ranked based on $(BH)_{max}$ values (as mentioned in Table 3).

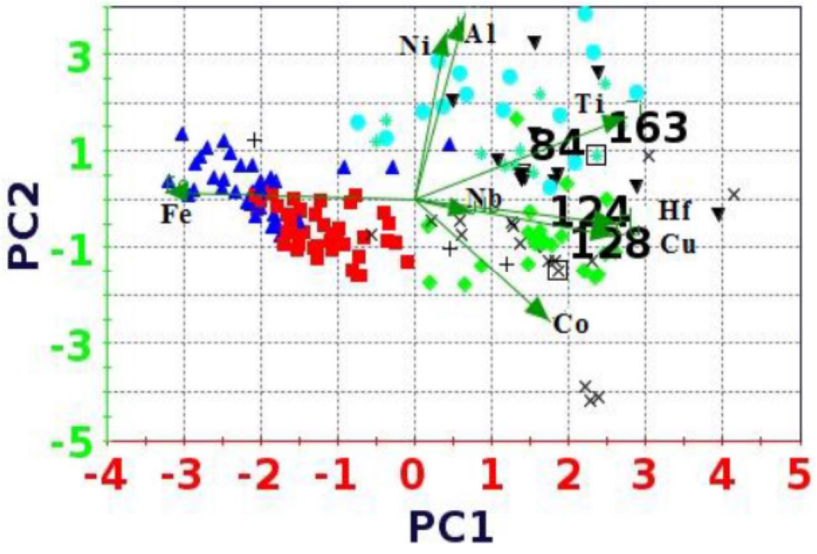

Fig. 25 Orientation of various elements in the PC space

From Fig. 25, one can observe that, Cu, Hf, Nb, and Fe contributes more towards PC1, of which Fe has the highest contribution. Ni and Al contribute more on PC2. Ti and Co has similar effect on both PC1 and PC2. Length and orientation of arrow are similar for Cu and Hf. Hence, Cu and Hf may affect the properties of alloy in the same manner. Similarly, length and orientation of arrows corresponding to Ni and Al suggests that these elements will affect the properties in the same way. One can observe that the marked alloys are clustered in a very small region while inferior alloys cover a majority of the PC space. Hence, if a certain alloy composition is near these top alloys in the PC space, then they can be given a chance over others during the selection of alloys for experimental validation.

Niobium has the lowest contribution towards PC1 while it is almost orthogonal to PC2. Hence, if we want to remove an element for rare-earth addition, we can reject Nb and manufacture a few alloys without it.

Thereafter, we used the dataset of 40 alloys selected by MCDM and did PC analysis on it. It was followed by cluster analysis on the dataset by K-means clustering (Kaufman approach) method. Based on D-B index, the data set was divided into 5 clusters. Alloys belonging to different clusters are denoted by different symbols.

In Fig. 26, one can see that the orientation of the arrows has been altered. This is expected as these alloys were selected by MCDM, and hence this reduced set will have different variance. A few alloys have been marked in Fig. 25 and Fig. 26. It can be observed that superior alloys are clustered together as alloys near these marked alloys were candidates that were part of the next set of alloys with superior properties. Hence, this method can be used for screening of the alloys prior to manufacture.

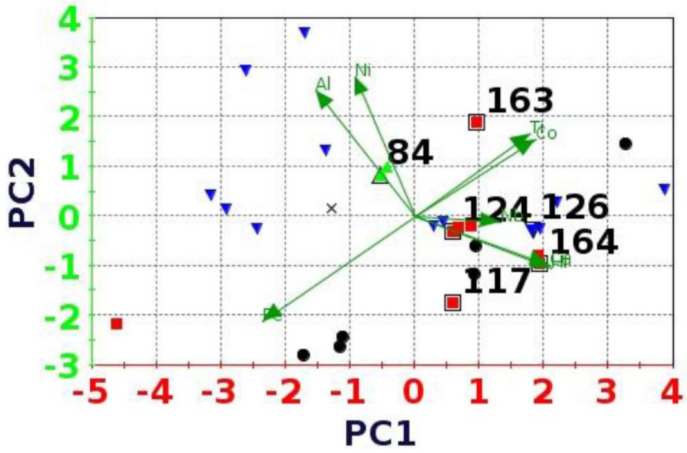

Fig. 26 Orientation of various elements in the PC space

In this set too, arrows corresponding to Cu and Hf overlap each other, which confirms our previous findings. Arrows corresponding to Ni and Al are oriented together as observed before. Nb is almost orthogonal to PC2 and, hence, has minimal effect on it. Nb is collinear to PC1, but length of arrow is smallest for Nb along PC1. His means that Nb will have least contribution. Therefore, one can

think of removing Nb from the next set of alloys and have it substituted with a rare-earth element. One peculiar finding is that Co and Ti are oriented together. This needs further investigation.

Hierarchical Cluster Analysis (HCA)

Clustering analysis is usually performed to find a pattern in a dataset. A cluster consists of data points which are similar to the other data points within the same cluster, while dissimilar to data points in the other clusters. In most cases, the similarity criterion is the Euclidian distance between the data points. In HCA, clustering begins with each data point within a cluster [9], [44]. These clusters are iteratively merged to form larger ones and finally merged into one large cluster. In this work, clustering was performed by Ward's approach while there are several other alternatives to this method [44,51]. The final result is a tree like structure referred to as "dendrogram", which shows the way the clusters are related. The user can specify a distance or number of clusters to view the dataset in disjoint groups. In this way, the user can eliminate a cluster that does not serve any purpose as per his expertise.

In this case, we used multivariate data analysis (MVA) node in optimization package: modeFRONTIER [44] and another statistical software known as IBM SPSS [51] for HCA analysis. The alloys were clustered on the basis of targeted properties. Dendrogram was cut in a manner so that it results in a total of 9 clusters (Cluster 0 to Cluster 8) as denoted by the numbers in the dendrogram plot. Figure 27 shows the dendrogram plot obtained from HCA analysis. Cluster 8 and cluster 7 were merged as one when analyzed by Ward's approach. Clustering parameters and the number of alloys included in each cluster have been tabulated in Table 6.

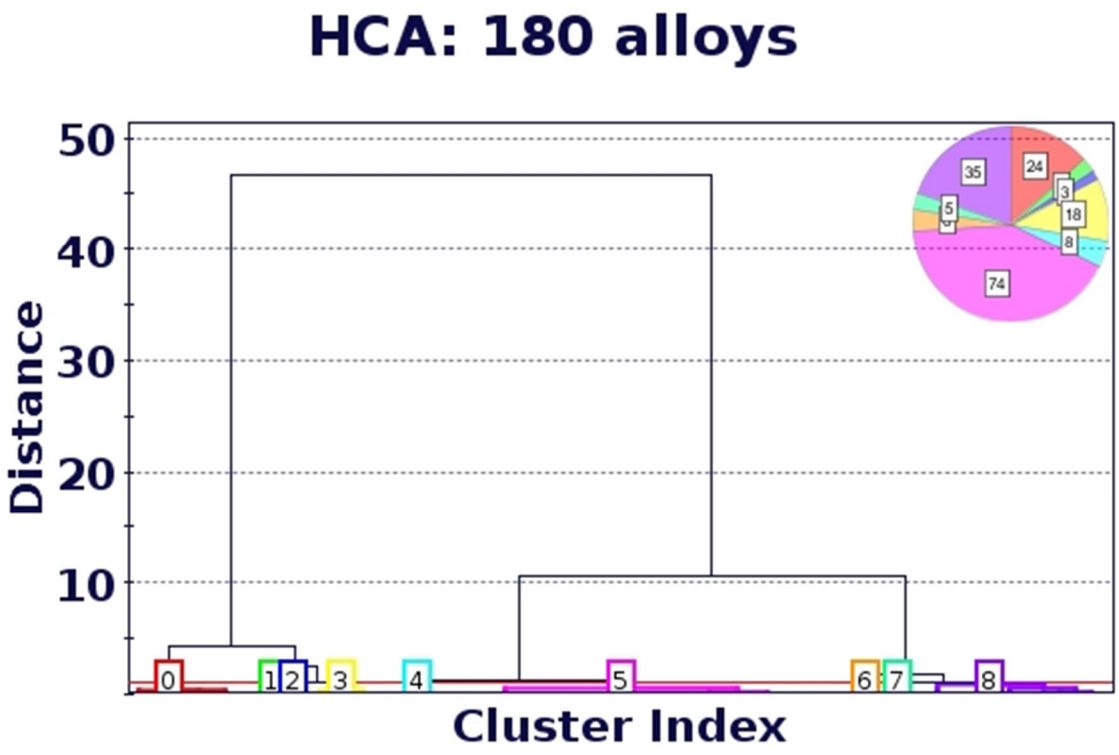

Fig. 27: Dendrogram plot from HCA analysis.

Clusters are classified by the following measures [44].

1. Internal similarity (ISim): It reflects the compactness of the *k*-th cluster. It must be higher.
2. External similarity (ESim): It reflects the uniqueness of *k*-th cluster. It must be lower.
3. Descriptive variables: These are the most significant variables that help in identifying cluster elements that are similar to one another.
4. Discriminating variables: These are the most significant variables that help in identifying cluster elements that are dissimilar to other clusters.

Table 6: Clustering parameters in HCA analysis

Cluster Number	Cluster Size	ISim	ESim	Best alloys
0	24	2.5	1.1	175,115
1	4	1.5	0.6	84, 86, 124, 139
2	3	1.5	0.7	145, 146, 147
3	18	3.2	0.8	117, 126, 128
4	8	4.5	1.3	
5	74	4.6	1.0	
6	6	1.7	1.0	
7	40	2.1	1.3	

From Table 6, we can see that cluster 1, cluster 2 and cluster 3 have higher Isim, while a lower Esim when compared to other clusters. Cluster 1 and cluster 3 contain top 10 alloys based on $(BH)_{max}$ value, while alloys in cluster 2 possess high H_c.

HCA analysis can be used to cross-check the findings of SVR analysis mentioned above in the text. The following text includes cluster scatter plots for various elements *versus* $(BH)_{max}$, H_c and B_r followed by relevant information extracted from them. In the following figures, confidence level for both the confidence interval and confidence ellipse is 0.9. These figures can be helpful in determining the variable bounds for targeted properties.

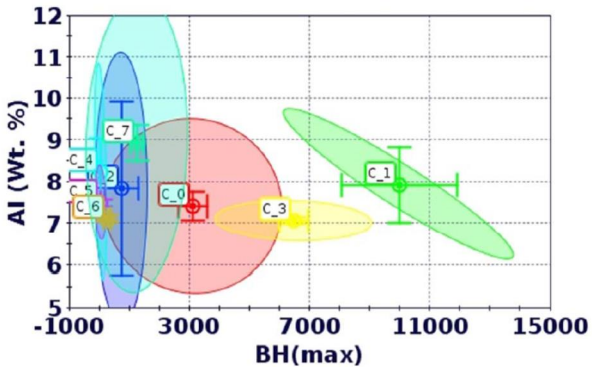

Fig. 28 Clusters scatter: (BH)max vs Al concentration

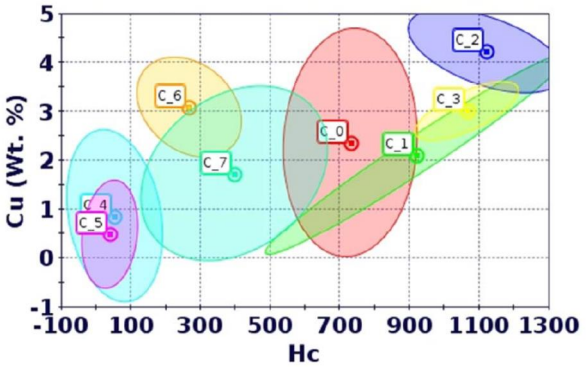

Fig. 29 Cluster scatter: Hc vs Cu concentration

In Fig. 28, for cluster 1, $(BH)_{max}$ increases with decrease in aluminum content in the range 6-10 wt. percent. Other clusters have mixed response for variation of aluminum.

It can be seen from Fig. 29 that H_c increases with an increase in Cu content in cluster 1 and cluster 3, while H_c, decreases with increasing Cu content in cluster 2 in a narrow composition range. Overall, copper affects H_c positively, and this is know from the literature as well as SVR analysis.

From Fig. 30, it is difficult to determine the role of Cu addition on B_r. From literature as well as SVR analysis, Cu tends to affect B_r positively. Hence, this needs further investigation.

Fig. 31 shows scatter plot for $(BH)_{max}$ *vs.* copper for various clusters. This behavior was expected as B_r and H_c are conflicting (see Figures 30 and 31). It is difficult to determine the role of Cu addition from $(BH)_{max}$ *vs.* Cu plot.

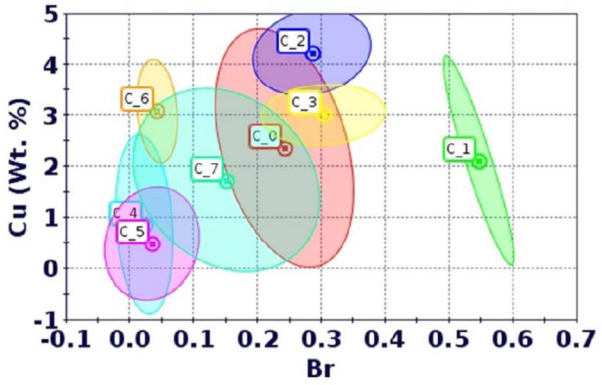

Fig. 30 Cluster scatter: Br vs Cu concentration

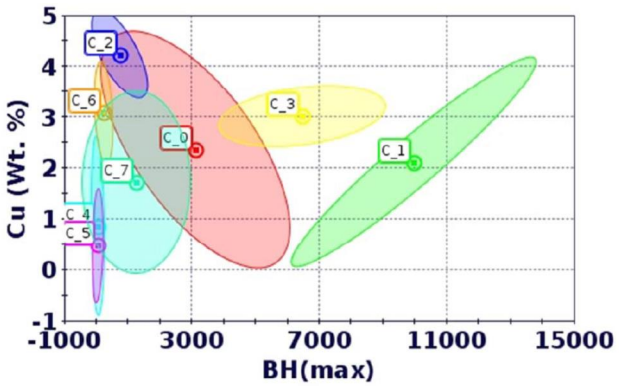

Fig. 31 Cluster scatter: (BH)max vs Cu concentration

From Fig. 32, one can observe that in cluster 2 and cluster 7, H_c tends to increase with an increase in Ti content.

From Fig. 33, it can be seen that in order to increase $(BH)_{max}$, one needs to stay in a narrow concentration range for Fe.
Nickel showed a weak response for $(BH)_{max}$ in SVR analysis. Hence, we plotted scatter plots for Ni *vs.* $(BH)_{max}$.

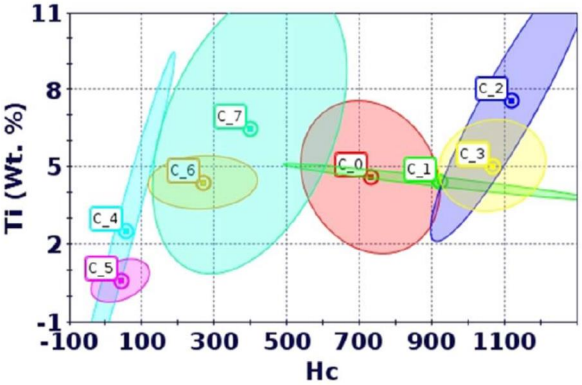

Fig 32 Cluster scatter: Hc vs Ti concentration

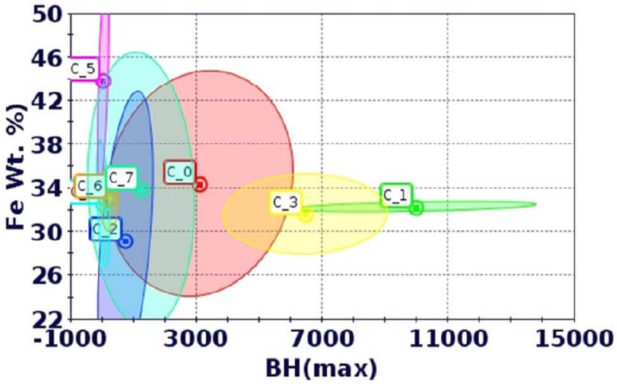

Fig. 33 Cluster scatter: (BH)max vs Fe concentration

From Fig. 34, it can be observed that in cluster 1, $(BH)_{max}$ increases with decrease in Ni content. This can also be observed in cluster 2.

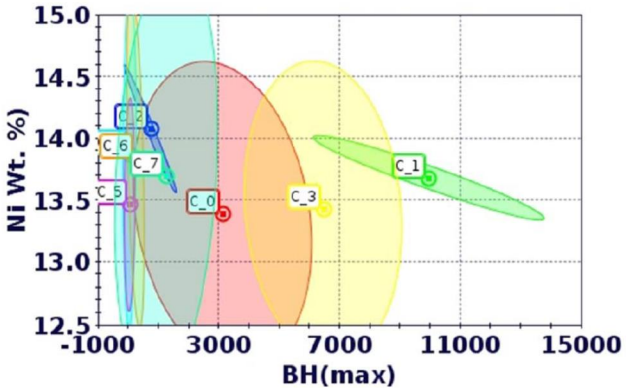

Fig. 34 Cluster scatter: (BH)max vs Ni concentration

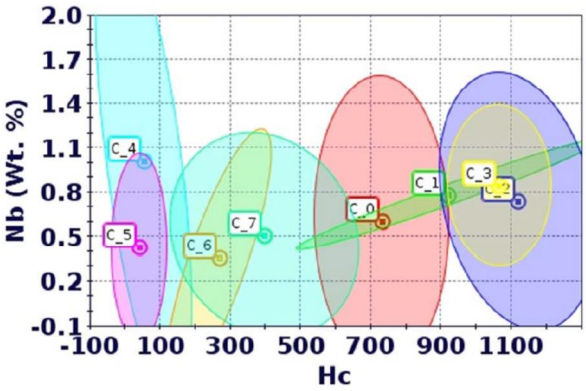

Fig. 35 Cluster scatter: Hc vs Nb concentration

One can also use these plots for discarding a few alloying elements in order to make way for REE addition. We plotted scatter plots for niobium *vs.* $(BH)_{max}$, H_c and B_r with this objective in mind.

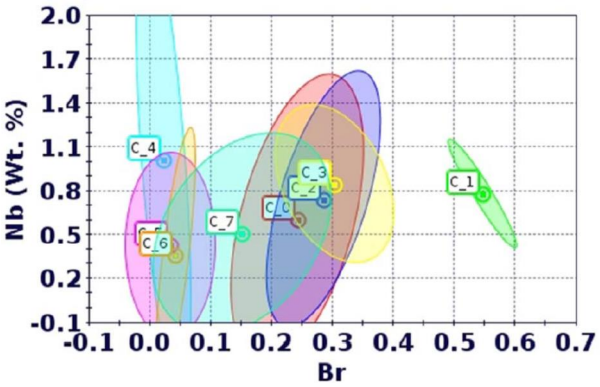

Fig. 36 Cluster scatter: Br vs Nb concentration

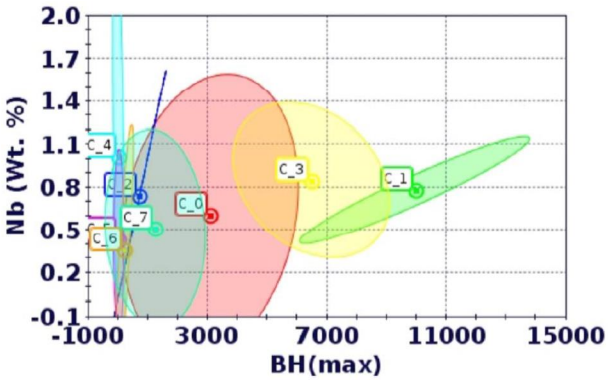

Fig. 37 Cluster scatter: (BH)max vs Nb concentration

From Figs. 35, 36 and 37, one can see that Nb is almost neutral to H_c and B_r. This was also observed in SVR analysis. Additionally, Nb has the same effect as Ti. Hence, one can think of manufacturing a few samples without Nb or replacing Nb with an affordable REE.

Thermodynamic Analysis

In this research, we have been using 8 alloying elements. Hence, it will be helpful for the experimentalists to have some information regarding the stability of critical phases during manufacture and designing heat treatment protocols. In this work, we studied phase stability of a few AlNiCo type alloys from 0°C to 1200°C using Factsage software [48]. The resulting diagrams are based on equilibrium calculation, hence the final experimental results may be different. However, these diagrams can be used as a guideline for the experimentalists when selecting alloys prior to manufacture [25,44].

From Fig. 38, it can be observed that alloy 124 is thermodynamically stable up to 800°C, while in alloys 84, 86 and 126 transformation (BCC-FCC) starts at a lower temperature. Hence, the experimentalists can design a heat treatment protocol so they can avoid transformations that will have a detrimental effect on the magnetic properties. We extended this analysis by modifying the composition of alloy 124. We added Mn in various amounts and plotted the critical phases.

From Fig. 39, it can be seen that these additions had detrimental effect and BCC-FCC transformation starting well below 800°C. Consequently, at this point we can say that AlNiCo type alloys should not have any Mn and B addition.

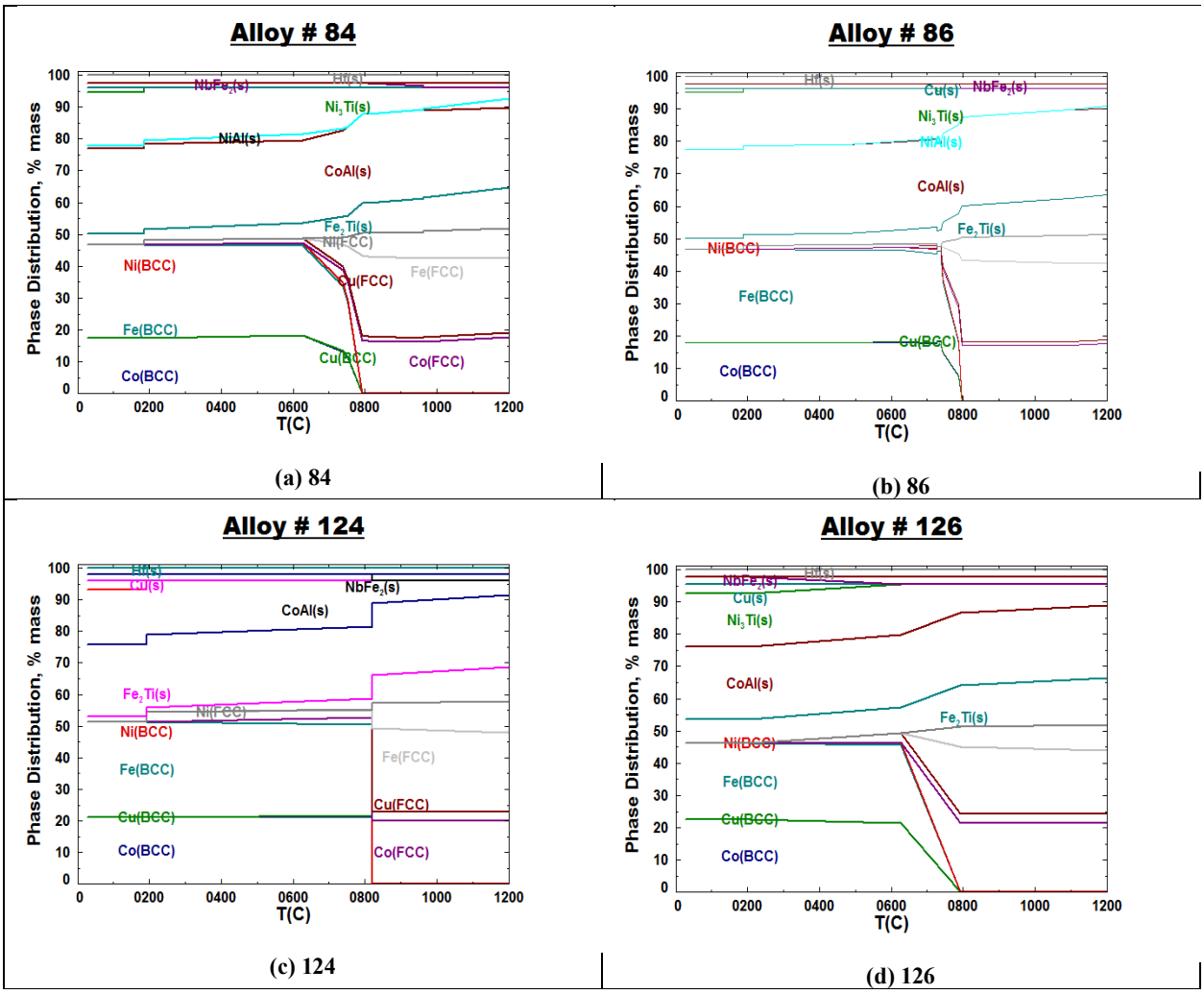

Fig. 38 Phase distribution diagrams for alloy (a) 84, (b) 86, (c) 124 and (d) 126.

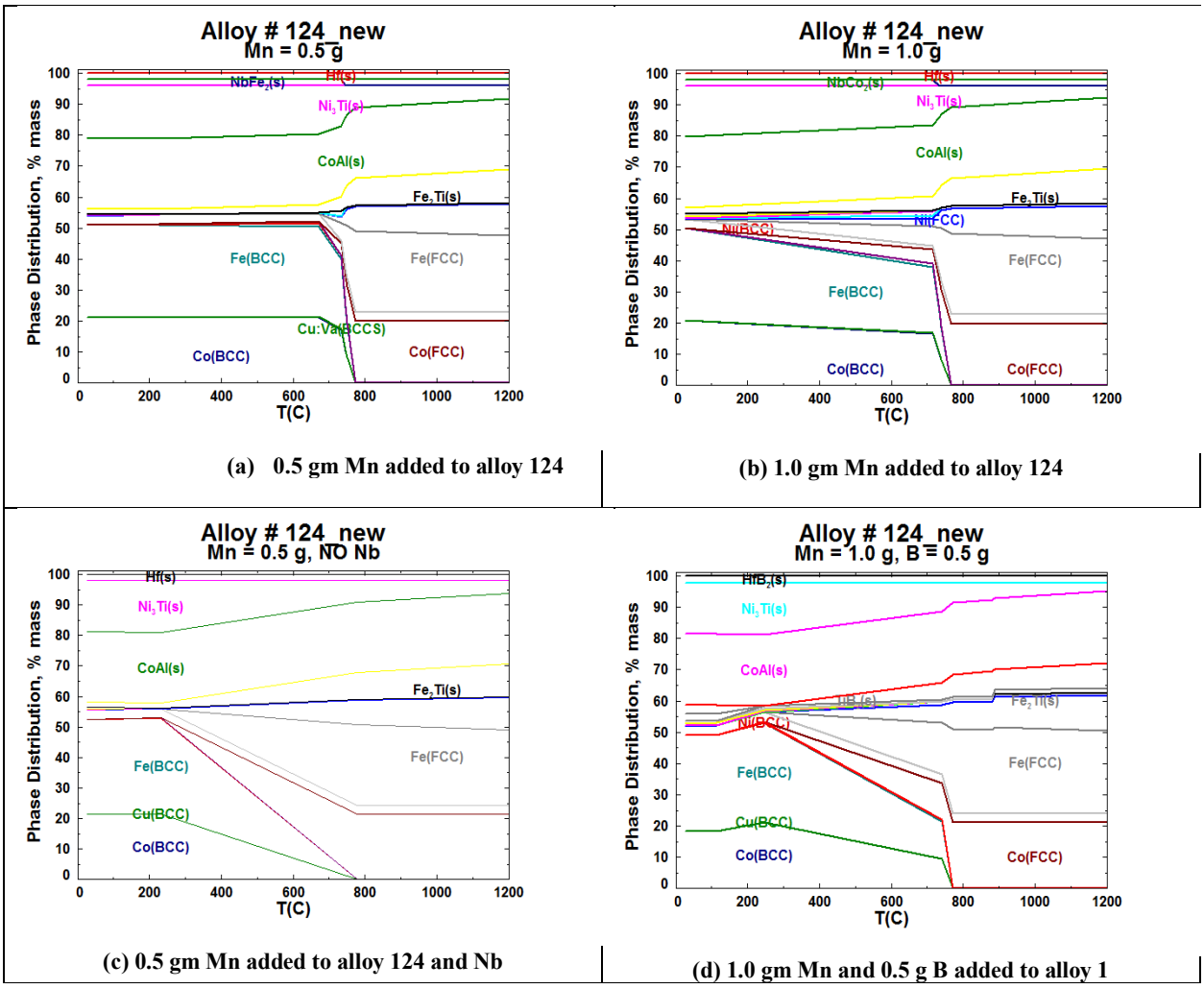

Fig. 39 Phase distribution diagram obtained after modifying composition of alloy 124 (a) 0.5 gm Mn added to alloy 124, (b) 1.0 gm Mn added to alloy 124, (c) 0.5 gm Mn added to alloy 124 and Nb removed, and (d) 1.0 gm Mn and 0.5 gm of B added to alloy 124.

Discussion

Figures 5, 6 and 7 show the scatter plots among magnetic energy density, magnetic coercivity, and magnetic remanence. Top 10 alloys are marked in these figures. In these figures as well as Table 6, alloys have been ranked on the basis of $(BH)_{max}$ values. At present, the best alloy is alloy number 124. From Figures 5, 6 and 7 one can observe that the Pareto-optimized alloys (modeFRONTIER and IOSO) dominate the initial 80 candidate alloys randomly predicted by Sobol's algorithm. One can observe from the figures that we were able to improve upon Hc without compromising on B_r.

In SVR, only Ni showed some weak/mixed response for $(BH)_{max}$. Hence, there is scope for improvement in the accuracy of the response surface algorithm. Copper was found to show a direct correlation with H_c and B_r. In this case, response surface predictions are at par with the literature. Hafnium shows positive correlation with H_c and B_r, which is promising, but needs further evaluation.

PC analysis proved to be helpful in reducing the dimensionality of the data set for visualization. PC analysis points towards a correlation between elements Cu-Hf and Ni-Al. Ni-Al rich phase is known in AlNiCo alloys and its effect on magnetic properties is supported by data from the literature. Hf has been rarely used in AlNiCo alloys and hence its similarity with Cu can be exploited to improve the magnetic properties. Hf enhances high temperature properties, hence the new magnets are supposed to have superior magnetic properties at elevated temperatures.

Special emphasis was on using a variety of data mining/pattern recognition statistical algorithms to elucidate relationships among different alloying elements and each of the desired magnetic properties of the alloys. Sensitivity analysis of the variation of concentrations of each of the alloying elements was performed revealing that some of the alloying elements have practically negligible influence on the three magnetic properties of the AlNiCo type alloys, while a few of the alloying elements cause significant changes in the macroscopic magnetic properties of such alloys.

From Figures 25 and 26, one can see that Nb has the lowest influence on PC1, although it is collinear to it. Niobium is almost orthogonal to PC2 and hence, it will have least contribution on it. This suggests that if one needs to exclude an element from further analysis, one can think of excluding Nb and manufacture a few samples without it. These findings are quite helpful in development of knowledge base for design of new materials. At the same time, it has the potential to save time and money otherwise invested in random experimentation.

PC analysis can be used as a tool to screen alloys predicted by various optimizers prior to manufacture. Alloys that are near to the previous best alloys in the PC space can be preferred for manufacture over the others for improved results.

At present, *ab-initio* based calculations, as well as Calphad [52] approach, are effective for limited systems (alloys having maximum 3-4 elements), and cannot handle eight alloying elements. Use of statistical tools will be helpful in determining the most influential alloying elements. This will be helpful in theoretical validation of the above findings. Additionally, one can work on finding the most stable phases needed for enhanced performance of these alloys by focusing on the most influential elements.

Recommendations for Future Research

Based on the obtained experimental verifications of the properties of the optimized magnetic alloys, it can be concluded that further efforts with optimization of chemical concentrations of the currently used alloying elements would not result in further improvements in magnetic properties.

However, research is highly recommended for determining which of the alloying elements could be replaced with small amounts of readily available, affordable rare earth elements so that (BH) max and Hc and Br could be significantly increased and maintained at higher temperatures.

The most promising direction for further research on developing new high performance magnetic alloys is optimization of parameters defining thermal treatment and magnetic treatment protocols. That is, optimizing temperature-time curve and applied magnetization field strength-time curve. To prove this point, tempering at 650 ^{0}C x 4 hrs + 600 ^{0}C x 6 hrs + 550 ^{0}C x 16 hrs, was added besides the standardized procedures. With this new procedure, H_c increased from 1100 Oe to 1350

Oe and $(BH)_{max}$ increased from 5600 J/m^3 to 6900 J/m^3 proving the importance and need for simultaneously optimizing chemistry and thermal treatment protocol.

The accuracy and robustness of the entire computational effort can be further improved by developing response surfaces that maintain high accuracy even outside the available experimental data set. The present alloy development time is approximately one year and it is significantly less than current alloy development cycle of about 10 years.

Acknowledgements

This work was partially funded by the US Air Force Office of Scientific Research under grant FA9550-12-1-0440 monitored by Dr. Ali Sayir. The Principal Investigator and CoInvestigators are grateful for this generous support and for the support from Prof. Igor N. Egorov and Prof. Carlo Poloni who contributed modeFrontier and IOSO software, respectively. The views and conclusions contained herein are those of the authors and should not be interpreted as necessarily representing the official policies or endorsements, either expressed or implied, of the US Air Force Office of Scientific Research or the U.S. Government. The U.S. Government is authorized to reproduce and distribute reprints for government purposes not withstanding any copyright notation thereon.

References

1. Constantinides S 2006 A manufacturing and performance comparison between bonded and sintered permanent magnets. Presented at APEEM, April 4, 2006
2. *Critical Materials Strategy*. 2010, US Department of Energy, http://www.energy.gov/news/documents/criticalmaterialsstrategy.pdf
3. P. Mcguiness, O. Akdogan, A. Asali, S. Bance, F. Bittner, J.M.D. Coey, N.M. Dempsey, J. Fidler, D. Givord, O. Gutfleisch, M. Katter, D. Le Roy, S. Sanvito, T. Schrefl, L. Schultz, C. Schwöbl, M. Soderžnik, S. Šturm, P. Tozman, K. Űstűner, M. Venkatesan, T.G. Woodcock, K. Žagar, S. Kobe, Replacement and Original Magnet Engineering Options (ROMEOs): A European Seventh Framework Project to Develop Advanced Permanent Magnets Without, or with Reduced Use of, Critical Raw Materials. JOM, 67, (2015) 1306–1317.
4. B.D. Cullity, C. Graham, Chapter 14. Hard magnetic materials. In: Introduction to Magnetic Materials, Second Edition, Wiley-IEEE Press, New York (2009) 477-504.
5. F. Ronning, S. Bader, Rare earth replacement magnets. Journal of Physics: Condensed Matter, 26, (2014) 1–3.
6. M.J. Kramer, R.W. McCallum, I.A. Anderson, S. Constantinides, Prospects for non-rare earth permanent magnets for traction motors and generators. JOM, 64, (2012) 752–763.
7. D.J. Sellmyer, B. Balamurugan, W.Y. Zhang, B. Das, R. Skomski, P. Kharel, Y. Liu, Advances in rare-earth-free permanent magnets. The 8th Pacific Rim International Congress on Advanced Materials and Processing (PRICM8), Waikoloa, Hawaii (4-9 August 2013).
8. L. Zhou, M. Miller, P. Lu, L. Ke, R. Skomski, H. Dillon, Q. Xing, A. Palasyuk, M. McCartney, D. Smith, S. Constantinides, R. McCallum, I. Anderson, V. Antropov, M. Kramer, Architecture and magnetism of alnico. Acta Materialia, 74, (2014) 224–233.
9. K. Rajan (eds), Materials informatics: An introduction. Informatics for Materials Science and Engineering: Data-Driven Discovery for Accelerated Experimentation and Application, 1st edition, Elsevier, (2013) 1–120.

10. M.F. Horstemeyer, Integrated Computational Materials Engineering (ICME) for Metals: Using Multiscale Modeling to Invigorate Engineering Design with Science. TMS - The Minerals, Metals and Materials Society, John Willey and Sons, Inc.), Hoboken, NJ (2012).
11. Jha, R., Dulikravich, G.S., Fan, M., Schwartz, J., Koch, C., Egorov, I.N., Poloni, C., "A Combined Computational-Experimental Approach to Design of High-Intensity Permanent Magnetic Alloys", CONEM214- *National Congress of Mechanical Engineering* (eds: Steffen, V., Bandarra, E., Rade, D.A.), Uberlandia, Brazil, August 10-15, 2014.
12. R. Jha, F. Pettersson, G.S. Dulikravich, H. Saxen, N. Chakraborti, Evolutionary design of nickel-based superalloys using data-driven genetic algorithms and related strategies. Materials and Manufacturing Processes, 30, 4, (2015) 488–510.
13. Dulikravich G S, Egorov I N, Sikka V K and Muralidharan G 2003 Semi-stochastic optimization of chemical composition of high-temperature austenitic steels for desired mechanical properties, *2003 TMS Annual Meeting, Yazawa International Symposium: Processing and Technologies* (eds: Kongoli F, Itakagi K, Yamaguchi C and Sohn H-Y) TMS Publication, San Diego, CA, March 2-6, 2003 **1** 801-814.
14. Yegorov-Egorov I N and Dulikravich G S 2004 Inverse design of alloys for specified stress, temperature and time-to-rupture by using stochastic optimization, Proceedings of *International Symposium on Inverse Problems, Design and Optimization – IPDO2004* (eds: Colaco M J, Orlande H R B and Dulikravich G S) Rio de Janeiro, Brazil, March 17-19.
15. Yegorov-Egorov I N and Dulikravich G S 2004 Optimization of alloy chemistry for maximum stress and time-to-rupture at high temperature, *10th AIAA/ISSMO Multidisciplinary Analysis and Optimization Conference; Paper AIAA-2004-4348* (eds: Messac A and Renaud J, AIAA, Albany, NY, Aug. 30 – Sept. 1, 2004.
16. Dulikravich G S and Egorov-Yegorov I N 2005 Design of alloy's concentrations for optimized strength, temperature, time-to-rupture, cost and weight, *Sixth International Special Emphasis Symposium on Superalloys 718, 625, 706 and Derivatives* (ed: Loria E A) TMS Publications, Pittsburgh, PA, October 2-5, 2005, 419-428.
17. Egorov-Yegorov I N and Dulikravich G S 2005 Chemical composition design of superalloys for maximum stress, temperature and time-to-rupture using self-adapting response surface optimization, *Materials and Manufacturing Processes* **20** (3) 569-590.
18. Dulikravich G S and Egorov-Yegorov I N 2005 Robust optimization of concentrations of alloying elements in steel for maximum temperature, strength, time-to-rupture and minimum cost and weight, *ECCOMAS – Computational Methods for Coupled Problems in Science and Engineering* (eds: Papadrakakis C, Onate E and Schrefler B) Fira, Santorini Island, Greece, May 25-28, 2005.
19. Dulikravich G S and Egorov I N 2006 Optimizing chemistry of bulk metallic glasses for improved thermal stability. Symposium on Bulk Metallic Glasses. *TMS 2006 Annual Meeting & Exhibition*, eds: Liaw, P. K. and Buchanan, R. A., San Antonio, TX, March 12-16, 2006.
20. Dulikravich G S, Egorov I N and Jelisavcic N 2006 Evolutionary optimization of chemistry of bulk metallic glasses, Proceedings of *III European Conference on Computational Solid and Structural Mechanics* (eds: Mota Soares C A, Martins J A C, Rodrigues H C, Ambrosio J A C, Pina C A B, Mota Soares C M, Pereira E R B and Folgado J), Springer, Lisbon, Portugal, June 5-8, 2006.
21. Dulikravich G S, Egorov I N and Colaco M J 2008 Optimizing chemistry of bulk metallic glasses for improved thermal stability, *Modelling and Simulation in Materials Science and*

Engineering, **16**, 075010-075029.
22. Dulikravich G S, Kumar A and Egorov I N 2008 Titanium based alloy chemistry optimization for maximum strength, minimum weight and minimum cost using JMatPro and IOSO software, *TMS Annual Meeting, Materials Informatics: Enabling Integration of Modeling and Experiments in Materials Science*, ed: Rajan, K., New Orleans, LA, March 9-13, 2008.
23. Bhargava S, Dulikravich G S, Murty G, Agarwal A and Colaco M J 2011 Stress corrosion cracking resistant aluminum alloys: Optimizing concentrations of alloying elements and tempering, *Materials and Manufact. Processes*, vol. 26, pp. 363-374.
24. Dulikravich, G. S. and Egorov, I. N., "Inverse Design of Alloys' Chemistry for Specified Thermo-Mechanical Properties by Using Multi-Objective Optimization", Chapter 8 in *Computational Methods for Applied Inverse Problems* (eds: Wang, Y. F., Yagola, A. G. and Yang, C. C.), Inverse and Ill-Posed Problems Series 56, Walter De Gruyter and Higher Education Press, P. R. China, ISBN: 978-3-11-025905-6, September 2012, pp. 197-219.
25. Thermocalc: http://www.thermocalc.com/solutions/by-application/alloy-development/, accessed on 3/1/2015 (2015).
26. R. Jha, F. Pettersson, G.S. Dulikravich, H. Saxen, N. Chakraborti, Evolutionary design of nickel-based superalloys using data-driven genetic algorithms and related strategies. Materials and Manufacturing Processes, 30, 4, (2015) 488–510.
27. R. Jha, G.S. Dulikravich, F. Pettersson, H. Saxen, N. Chakraborti, A combined experimental-computational approach to design optimization of high temperature alloys. In: ASME Symposium on Elevated Temperature Application of Materials for Fossil, Nuclear, and Petrochemical Industries, ASME, Seattle, WA (March 25-27, 2014).
28. R. Rettig, N.C. Ritter, H.E. Helmer, S. Neumeier, R.F. Singer, Single-crystal nickel-based superalloys developed by numerical multi-criteria optimization techniques: design based on thermodynamic calculations and experimental validation. Modelling and Simulation in Materials Science and Engineering, 23, 3, (2015) 035004.
29. I. Toda-Caraballo, P.E.J. Rivera-Diaz-Del-Castillo, Modelling and design of magnesium and high entropy alloys through combining statistical and physical models. JOM, 67, 1 (2015) 108–117.
30. N. Settouti, H. Aourag, A study of the physical and mechanical properties of lutetium compared with those of transition metals: A data mining approach. JOM, 67, 1 (2015) 87–93.
31. T. Mueller, A. Kusne, R. Ramprasad, Machine learning in materials science: Recent progress and emerging applications. Reviews in Computational Chemistry, 29 (2016).
32. A.G. Kusne, T. Gao, A. Mehta, L. Ke, M.C. Nguyen, K.M. Ho, V. Antropov, C.Z. Wang, M.J. Kramer, C. Long, I. Takeuchi, On-the-fly machine-learning for high-throughput experiments; search for rare-earth-free permanent magnets, Scientific Reports 4 published online (15 September 2014) article no. 6367, doi:10.1038/srep06367.
33. H. Dilon, Effects of heat treatment and processing modifications on microstructure in alnico-8H permanent magnetic alloys for high temperature applications. Graduate thesis and dissertations, Iowa State University, http:/lib.dr.iastate.edu/etd/13867 (2014), paper 13867.
34. Q. Xing, M.K. Miller, L. Zhou, H.M. Dillon, R.W. McCallum, I. Anderson, S. Constantinides, M.J. Kramer, Phase and elemental distributions in alnico magnetic materials. IEEE Transactions on Magnetics, 49, 7, (2013) 3314–3317.

35. R. Jha, G.S. Dulikravich, M.J. Colaco, M. Fan, J. Schwartz, C.C. Koch, Magnetic alloys design using multi-objective optimization, to appear in Advanced Structured Materials series (eds.: Oechsner, A., da Silva, L.M., Altenbach, H.), Springer, Germany (2016).
36. R. McCallum, L. Lewis, R. Skomski, A. Kramer, I.A. Anderson, Practical aspects of modern and future permanent magnets. Annual Review of Materials Research, 44, 1, (2014) 451–477.
37. Eringen, A.C., and Maugin, G.A., 1990, *Electrodynamics of Continua II; Fluids and Complex Media*, pp. 27, Springer-Verlag, New York.
38. Johnk, C.T.A., 1988, *Engineering Electromagnetic Fields and Waves*, pp.133, John Wiley and Sons, New York.
39. Cottingham, W.N., and Greenwood, D.A., 1991, *Electricity and Magnetism*, pp. 94, Cambridge University Press, Cambridge.
40. N. Makino, Y. Kimura, Techniques to achieve texture in permanent magnet alloy systems, Journal of Applied Physics, 36(3), (1965) 1185–1190.
41. S. Pramanik, V. Rao, O.N. Mohanity, Effect of niobium on the directional solidification and properties of alnico alloys, Journal of Materials Science, 28, (1993) 1237-1244.
42. I.M. Sobol, Distribution of points in a cube and approximate evaluation of integrals. U.S.S.R. Comput. Maths. Math. Phys, 7, (1967) 86-112.
43. Dulikravich, G. S. and Colaco, M. J., "Hybrid Optimization Algorithms and Hybrid Response Surfaces", Chapter 2 in *Advances in Evolutionary and Deterministic Methods for Design, Optimization and Control in Engineering and Sciences* (eds.: D. Greiner, B. Galván, J. Periaux, N. Gauger, K. Giannakoglou, G. Winter), Computational Methods in Applied Sciences Series, Springer Verlag, 2015, pp. 19-47. ISBN: 978-3-319-11541-2
44. ESTECO: modeFRONTIER, http://www.esteco.com/modefrontier, accessed on 3/1/2015 (2015).
45. Egorov I N 1998 Indirect optimization method on the basis of self-organization. Proceedings of *Optimization Techniques and Applications (ICOTA'98),* Curtin University of Technology, Perth, Australia **2** 683-691.
46. K. Deb, *Multi-objective optimization using evolutionary algorithms*. John Wiley and Sons, Chichester, UK (2001).
47. Colaco, M.J., Dulikravich, G.S. and Sahoo, D., A Response Surface Method-Based Hybrid Optimizer, *Inverse Problems in Science and Engineering*, Vol. 16, No. 6, 2008, pp. 717-741.
48. Factsage, http://www.factsage.com/, accessed on 3/1/2015 (2015).
49. F. Pettersson, N. Chakraborti, H. Saxen, A genetic algorithms based multi-objective neural net applied to noisy blast furnace data. Applied Soft Computing, 7, 1, (2007) 387–397.
50. B.K. Giri, J. Hakanen, K.Miettinen, N. Chakraborti, Genetic programming through bi-objective genetic algorithms with a study of a simulated moving bed process involving multiple objectives. Applied Soft Computing Journal, 13, 5, (2013) 2613–2623.
51. IBMSPSS: IBM corp. released 2013. IBM spss statistics for windows, version 22.0. armonk, ny: Ibm corp., http://www-01.ibm.com/software/analytics/spss/, accessed on 3/1/2015 (2015).
52. P.J. Spencer, A brief history of {CALPHAD}. Calphad, 32, 1, (2008) 1–8.

Appendix A: The chemical compositions of 180 alloys that were manufactured and tested

	X1	X2	X3	X4	X5	X6	X7	X8
Alloy number	Concentrations (percent)							
	Fe	Co	Ni	Al	Ti	Hf	Cu	Nb
1	48.7325	27.7207	14.0393	8.1985	0.2553	0.3941	0.0403	0.6194
2	46.2891	30.2861	13.1307	7.0275	1.3609	1.0282	0.5350	0.3424
3	36.1599	39.7725	13.2535	8.0599	0.7813	1.7003	0.0392	0.2333
4	41.4348	35.9678	13.1705	7.8148	0.3531	0.3927	0.1417	0.7245
5	34.3442	39.9990	13.6666	8.5062	0.1526	0.2230	1.1378	1.9706
6	47.6602	28.8599	14.1400	7.3723	0.3293	1.1736	0.0482	0.4167
7	43.1247	33.5122	13.0233	7.2595	0.4585	0.3230	1.9041	0.3947
8	49.5202	27.3384	13.2598	7.6967	0.9725	0.6519	0.0958	0.4648
9	45.4991	31.8735	13.1968	7.7978	0.5424	0.3452	0.6861	0.0590
10	41.4315	36.1577	13.1008	7.1119	0.2970	0.5491	0.6396	0.7125
11	29.2160	39.9995	14.9999	7.2552	4.1303	4.1105	0.2053	0.0833
12	45.8854	31.0237	13.1220	7.8935	0.7933	0.5915	0.1292	0.5615
13	51.4362	24.9612	14.1142	7.4326	0.3304	0.1286	0.9495	0.6474
14	38.9533	38.1936	13.3947	7.3020	1.2282	0.5500	0.2823	0.0959
15	46.6094	29.7747	13.3072	7.6165	1.4804	0.3441	0.2350	0.6327
16	44.9419	32.4719	13.2674	7.2901	0.4803	0.6093	0.6298	0.3092
17	41.0125	36.9446	13.2054	7.2037	1.0339	0.3026	0.0834	0.2140
18	39.4787	37.2195	13.3815	7.0086	0.2303	1.4124	0.2619	1.0071
19	42.9125	33.9304	13.3415	7.5056	1.4223	0.3902	0.4055	0.0921
20	48.5265	28.3152	13.3661	7.3394	0.4145	1.0276	0.0371	0.9737
21	52.5361	24.8503	13.1772	7.1582	0.8446	0.3506	0.5805	0.5025
22	42.1357	35.1814	13.0271	7.9691	0.5963	0.1428	0.7215	0.2260
23	37.9445	39.6541	13.4612	7.5253	0.1623	0.8236	0.1781	0.2509
24	46.7045	29.4490	13.1929	7.4621	0.7747	0.1515	1.9381	0.3273
25	35.8737	39.8669	13.0830	7.8805	0.3523	1.4379	1.0431	0.4626
26	42.7426	34.0626	13.7422	7.5586	0.7946	0.7035	0.2161	0.1797
27	49.1088	27.5118	13.0650	8.5767	0.3838	0.3390	0.1707	0.8443
28	52.5778	24.2325	14.1043	7.6306	0.4774	0.5386	0.1626	0.2761
29	44.9535	32.4562	13.2306	8.2626	0.1316	0.5555	0.0297	0.3803
30	47.0941	29.4327	13.8957	7.1327	0.4904	0.4976	0.5248	0.9320
31	47.5144	29.0460	13.2858	7.3207	1.3332	0.3838	0.8544	0.2616
32	35.3972	39.9835	13.1686	7.2191	0.3149	0.7850	2.0966	1.0350
33	45.0088	31.8912	14.1595	7.4270	0.1748	0.4014	0.6495	0.2878

34	49.2065	27.4264	14.3446	7.0749	0.6088	1.0823	0.0680	0.1887
35	44.2343	33.2760	13.9864	7.2397	0.4323	0.1748	0.3089	0.3476
36	47.6505	28.9049	13.2242	7.9931	0.4496	1.4883	0.1171	0.1723
37	39.1697	37.8112	13.5484	7.2627	0.8662	0.7322	0.4803	0.1293
38	38.5661	39.0641	13.0734	7.1822	0.2042	1.2573	0.0691	0.5836
39	36.6916	39.6696	13.0368	8.5587	0.5726	0.3836	0.6565	0.4307
40	46.1031	30.4723	13.1831	7.4783	0.5138	0.6256	0.1943	1.4295
41	35.4775	39.9215	13.5019	8.4017	0.6816	0.2611	0.1460	1.6087
42	39.8271	37.0863	13.6299	7.4209	0.1296	0.9761	0.2984	0.6318
43	43.0087	33.6215	13.8198	7.0854	0.6831	0.4225	0.5137	0.8452
44	45.5297	31.2406	14.0217	7.2727	0.9117	0.1573	0.0809	0.7854
45	42.6312	35.2279	13.1725	7.1224	0.2072	0.3362	0.9492	0.3534
46	46.3754	30.8822	13.5414	7.7311	0.3702	0.7518	0.2512	0.0968
47	39.5371	38.0009	13.4167	7.1883	0.1380	0.1474	0.4356	1.1360
48	45.9401	31.0712	13.2106	7.0154	0.2576	0.3827	1.2002	0.9222
49	45.1891	31.4657	13.5998	7.4378	1.5286	0.5004	0.0269	0.2518
50	40.6930	36.1425	13.4012	8.0854	0.4461	0.6185	0.0192	0.5942
51	51.9264	25.2440	13.7225	7.4653	0.3034	0.6841	0.5612	0.0932
52	47.7037	29.7167	13.7815	7.0370	0.7335	0.2540	0.3429	0.4306
53	37.3318	39.6132	14.4244	7.1525	0.5397	0.8799	0.0331	0.0256
54	39.9593	36.8983	13.1182	7.8259	0.5069	0.1103	1.2475	0.3337
55	25.7095	39.9999	14.0001	8.9440	5.0548	3.1384	1.5492	1.6042
56	45.0877	32.3223	13.7122	7.3225	0.9449	0.3447	0.1901	0.0754
57	50.8326	25.7559	13.0974	8.3054	0.2487	0.7131	0.1506	0.8962
58	40.3220	36.8575	13.7762	7.1755	0.3914	0.6553	0.4055	0.4168
59	46.6644	30.6451	13.1922	7.1394	0.3072	1.8470	0.1372	0.0676
60	37.8433	39.5513	13.5164	7.6198	0.7547	0.1034	0.5005	0.1105
61	41.0032	35.6275	13.1261	8.3344	1.4095	0.2008	0.2800	0.0185
62	46.5526	30.8736	13.3219	7.2685	0.4895	0.2452	1.0960	0.1528
63	43.6681	33.3785	13.4448	8.1756	0.6134	0.4472	0.1046	0.1678
64	41.6868	35.6136	13.3149	7.1313	0.1789	0.6588	0.3508	1.0649
65	43.8697	33.0091	13.2780	7.6478	0.2449	1.5792	0.0531	0.3182
66	52.3517	24.1653	13.9459	7.0970	0.8158	0.8232	0.4398	0.3612
67	44.0016	32.9305	13.2165	7.0389	1.3363	0.4126	0.8153	0.2483
68	44.6086	32.5438	13.6056	7.4768	0.2003	0.5920	0.3949	0.5779
69	47.0044	30.1629	14.3100	7.1641	0.4675	0.2342	0.1466	0.5103
70	34.3054	39.9988	13.1000	7.2862	0.7490	1.8196	1.7843	0.9566

71	42.9968	34.1815	13.4022	7.4399	0.6820	0.1662	1.0618	0.0697
72	38.7243	38.6541	13.0862	7.0585	0.1246	0.7236	1.2215	0.4071
73	37.0351	39.9846	13.0098	7.0391	1.4901	0.1936	0.4215	0.8262
74	51.3183	26.2600	13.0325	7.8655	0.5286	0.7289	0.0268	0.2395
75	36.2859	39.8889	13.8035	7.1209	0.4843	1.9189	0.2099	0.2879
76	44.1377	33.7082	13.1405	7.0509	0.2803	0.9984	0.1677	0.5163
77	52.8601	25.0788	13.2923	7.4367	0.6446	0.2701	0.1218	0.2956
78	35.7951	39.9616	14.0921	7.8361	0.2396	0.1659	0.2243	1.6853
79	37.2232	39.4340	14.7026	7.0913	0.1363	0.2916	0.2680	0.8530
80	39.9487	36.8422	13.7258	8.1467	0.2279	0.5858	0.2541	0.2688
81	29.7440	39.7627	14.4601	8.9994	0.5707	2.8016	2.3394	1.3221
82	39.6668	35.0850	13.0256	8.1331	0.8769	0.6107	2.5888	0.0131
83	42.1118	30.9983	13.7041	8.4617	1.9713	0.4794	1.5261	0.7473
84	32.4409	35.7158	13.8133	8.7424	4.6165	2.6559	1.3867	0.6286
85	47.0940	29.4330	13.8960	7.1330	0.4900	0.4976	0.5248	0.9328
86	31.9210	36.5730	13.8240	8.5740	4.7620	2.5363	1.1804	0.6295
87	31.8760	36.4750	13.8730	8.5730	4.7400	2.5858	1.2364	0.6402
88	45.2740	29.4050	13.6490	7.0000	4.0000	0.1015	0.5694	0.0003
89	39.6700	32.1040	14.3790	7.0000	4.0000	1.6334	0.7165	0.4973
90	33.0210	35.1330	14.9790	9.7830	5.0260	0.9693	0.9813	0.1084
91	38.7266	28.4688	13.6563	8.3281	6.7344	1.8672	1.8281	0.3906
92	30.8205	32.4727	13.3164	10.6426	8.2793	2.3713	1.4824	0.6816
93	29.4022	37.0332	14.6738	10.6279	5.6885	0.1028	1.9834	0.4521
94	30.3679	35.4707	13.9863	7.0342	9.4072	2.7310	0.5771	0.4209
95	32.3595	36.8574	13.5449	7.2002	4.1162	2.0683	2.9385	0.9307
96	35.9806	28.3418	13.4668	10.9111	9.8584	0.3690	0.6182	0.4697
97	35.9051	28.0146	13.7334	8.8823	7.2368	2.8032	2.4683	0.9692
98	37.8364	28.6396	13.8584	9.8198	5.9243	2.2594	1.1558	0.4067
99	33.4307	33.1904	13.8701	10.3765	6.9771	1.0077	0.9155	0.2056
100	33.4609	30.3877	14.7939	8.4771	7.7632	1.9677	2.6938	0.4292
101	32.0125	32.4189	14.8877	11.0552	5.2476	2.9193	0.6782	0.7886
102	36.8406	31.4814	13.0752	11.5239	4.1538	0.4724	2.0845	0.3823
103	38.5908	31.4229	13.2900	9.6782	5.2339	0.8746	0.7896	0.1069
104	35.2111	32.2041	13.7588	10.0688	6.4370	0.5574	1.6802	0.0601
105	40.7634	28.6885	14.3682	7.9204	5.6167	0.8519	1.3286	0.5366
106	31.1751	37.8267	13.1401	10.7000	4.0940	2.5363	0.4475	0.0432
107	40.8464	29.4917	13.3345	9.9358	4.7742	0.9319	0.1326	0.6501
108	24.0687	37.8901	13.7954	11.9084	7.4265	1.7362	2.5583	0.5681
109	34.1474	31.5034	13.9321	9.9651	5.9636	1.7192	1.9548	0.7419
110	41.0275	28.1831	13.8931	7.5627	7.0847	0.3032	1.5681	0.3474

111	32.3595	36.8574	13.5449	7.2002	4.1176	2.0683	2.9385	0.9307
112	32.4349	35.7235	13.8130	8.7408	4.6193	2.6544	1.3845	0.6286
113	32.4409	35.7158	13.8133	8.7424	4.6169	2.6260	1.3867	0.6286
114	32.3333	36.8574	13.5449	7.2052	4.1162	2.0683	2.9385	0.9307
115	31.4554	38.0000	13.3020	7.0000	4.2426	3.0000	3.0000	0.0000
116	40.7793	28.2932	13.0288	7.3842	4.0449	3.0000	2.9945	0.4751
117	35.2810	33.8728	13.0000	7.0000	4.0000	2.9640	2.8821	1.0000
118	34.5512	34.9514	13.3825	7.0000	4.1149	3.0000	3.0000	0.0000
119	39.7243	30.2015	13.0742	7.0000	4.0000	3.0000	3.0000	0.0000
120	42.0311	28.0000	13.1323	7.0000	4.0000	2.8696	2.9670	0.0000
121	32.4409	35.7158	13.8133	8.7424	4.6165	2.6559	1.3867	0.6286
122	31.9210	36.5730	13.8240	8.5740	4.7620	2.5363	1.1804	0.6295
123	35.2810	33.8728	13.0000	7.0000	4.0000	2.9640	2.8821	1.0000
124	32.3342	36.8574	13.5449	7.2055	4.1255	2.0683	2.9385	0.9307
125	28.5910	37.9233	13.4081	7.0033	6.4618	2.9598	2.6544	0.9982
126	29.9279	37.9150	13.0021	7.0721	5.7514	2.3725	2.9594	0.9996
127	29.9425	36.5839	13.1237	7.3165	6.0832	2.9797	2.9990	0.9714
128	31.1017	38.0000	13.0000	7.0002	5.1187	2.7819	2.9970	0.0005
129	30.0204	30.5200	14.0720	8.3281	10.8906	2.6920	2.6800	0.7969
130	34.2118	30.8125	13.5625	7.4700	10.2400	0.7344	2.2500	0.7188
131	26.0756	34.7188	13.7812	11.9219	10.6719	1.9000	0.2900	0.6406
132	26.6587	37.3750	13.1250	9.5400	10.3500	1.0063	1.0880	0.8570
133	31.4226	28.1562	14.5938	11.5500	8.7031	2.4109	2.4290	0.7344
134	27.7454	33.9375	14.9375	8.7188	10.3438	2.1650	2.0320	0.1200
135	29.6004	35.9688	13.0312	8.7969	8.9600	1.4141	1.7130	0.5156
136	30.3885	35.6562	14.0938	8.0156	9.1100	0.2359	2.0156	0.4844
137	32.5155	34.5625	14.3125	7.2700	7.4300	1.0969	2.7188	0.0938
138	27.3796	35.0900	14.7370	9.9700	8.8000	2.7734	0.8906	0.3594
139	32.3350	36.8880	13.5450	7.2060	4.1260	2.0680	2.9390	0.9310
140	32.4500	35.6950	13.8120	8.7420	4.6170	2.6580	1.3890	0.6280
141	32.4280	35.7130	13.8370	8.7420	4.5020	2.6560	1.3790	0.6810
142	32.4410	35.7050	13.8130	8.7430	4.6170	2.6580	1.3900	0.6290
143	31.7370	37.0130	13.4240	7.1940	4.8200	2.0820	2.9200	0.8920
144	28.2190	34.8110	13.7950	9.7780	5.4420	3.3010	4.2190	0.4050
145	24.2910	36.9620	14.3290	7.4060	7.9230	4.2880	4.4480	0.2900
146	36.3370	28.7810	14.0470	9.5530	4.8600	1.1830	4.4760	0.8610
147	26.9150	33.4680	13.8480	6.6160	9.9050	4.3280	3.7710	1.0760
148	29.8490	38.2560	13.1750	7.4220	4.5260	2.6930	4.1030	0.0230
149	40.4470	29.0050	13.0340	6.0000	4.0430	2.6800	3.9240	0.8480
150	32.3560	30.9440	14.0790	6.3440	8.5030	2.1660	4.1920	1.3520
151	32.1215	37.5812	13.7635	7.2151	4.0000	1.8435	2.7685	0.7067

152	32.0610	37.6190	13.6990	7.1500	4.0000	1.8820	2.7970	0.7920
153	32.1670	37.2670	13.5507	7.1680	4.2390	1.8762	2.8935	0.8387
154	32.3501	37.8487	13.8615	7.2665	4.0285	1.8566	2.7882	0.0000
155	32.3170	37.9193	13.8084	7.2071	4.0319	1.8970	2.8193	0.0000
156	34.0000	35.0000	15.0000	7.0000	5.0000	0.0000	4.0000	0.0000
157	29.0000	38.0000	14.0000	8.0000	8.0000	0.0000	3.0000	0.0000
158	35.5000	35.4000	13.1000	7.0000	5.0000	0.0000	3.2000	0.5000
159	49.9000	24.3000	14.0000	8.2000	0.0000	0.0000	2.3000	1.0000
160	30.0000	40.1000	13.0000	7.1000	6.5000	0.0000	3.0000	0.0000
161	31.9700	36.9350	13.5390	7.2370	4.2440	2.0640	2.9440	0.9360
162	33.3460	34.8990	13.0440	6.8430	5.3360	2.5760	3.4760	0.4800
163	29.2020	36.6050	15.3500	6.7780	5.8560	1.8980	3.4430	0.8680
164	31.1230	36.3650	13.0670	6.6370	5.4720	2.9420	3.4820	0.9110
165	30.5780	36.9230	13.0240	6.9540	5.2520	2.9070	3.4180	0.9440
166	29.9918	37.8933	13.0104	7.0837	5.7168	2.3338	2.9561	1.0113
167	33.9403	33.9776	13.9462	6.7076	5.8259	2.5400	2.4587	0.5954
168	32.3063	36.8503	13.5243	7.2180	4.1481	2.0814	2.9326	0.9467
169	32.2000	36.8000	13.6000	7.5000	4.1000	2.1000	2.8000	0.9000
170	32.2000	36.0000	13.6000	7.3000	4.2000	2.7000	3.1000	0.9000
171	28.3258	42.9837	11.6459	6.0053	5.2089	3.0903	2.5562	0.1828
172	27.2778	43.7572	11.5374	5.8714	5.6947	2.9807	2.5757	0.3011
173	28.5000	42.6932	11.5513	5.4903	5.7343	3.2785	2.5040	0.2468
174	33.5636	39.8291	12.6399	6.7627	4.1389	0.5997	1.7601	0.7234
175	33.3008	39.5205	12.7374	6.6623	4.2653	0.5627	1.8941	1.1064
176	33.0645	39.5244	12.6955	6.9787	5.1602	0.5141	1.8038	0.2878
177	33.1785	39.3977	12.5992	6.6029	4.5547	0.8510	1.7121	1.1311
178	32.7714	39.4603	12.6742	6.9077	5.0429	0.6910	1.9384	0.5110
179	33.1529	39.4522	12.6622	6.7129	4.5150	0.5629	1.8533	1.1082
180	32.3350	36.8880	13.5450	7.2060	4.1260	2.0680	2.9390	0.9310

List of Publications, Presentations and Dissertations Resulting from this Project

List of publications acknowledging the AFOSR grant FA9550-12-1-0440 support:

1. Dulikravich, G.S. and Colaco, M.J., "Hybrid Optimization Algorithms and Hybrid Response Surfaces", a chapter in Advances in Evolutionary and Deterministic Methods for Design, Optimization and Control in Engineering and Science (*eds.: D. Greiner, B. Galván, J. Periaux, N. Gauger, K. Giannakoglou, G. Winter*), *Computational Methods in Applied Sciences Series*, Springer Verlag, 2015, pp. 19-47. ISBN: 978-3-319-11541-2 DOI: 10.1007/978-3-319-11541-2_2

Journal articles published

1. Jha, R., Dulikravich, G.S., Pettersson, F., Saxén, H., Chakraborti, N., "Evolutionary Design of Nickel Based Superalloys Using Data-driven Genetic Algorithms and Related Strategies", *Materials and Manufacturing Processes, 2015,* http://dx.doi.org/10.1080/10426914.2014.984203**.**

Conference papers published

1. Jha, R., Dulikravich, G.S., Colaco, M.J., "Design and Optimization of Magnetic Alloys and Nickel-Based Superalloys for High Temperatures Applications", COBEM-2015, paper 1284, Rio de Janeiro, Brazil, December 6-11, 2015.
2. Jha, R., Dulikravich, G.S., Colaco, M.J., Egorov. I.N., Poloni, C., Chakraborti, N., Fan, M., Schwartz, J.and Koch, C.C., "Multi-Objective Design and Optimization of Hard Magnetic Alloys Free of Rare Earths", MS&T15-Materials Science and Technology 2015 Conference, Columbus, Ohio, October 4-8, 2015.
3. Dulikrvich, G.S., Reddy, S., Orlande, H.R.B. and Colaco, M.J., "Inverse Determination of Diffusion Coefficients in Arbitrary Objects Creating Desired Non-isotropy of Field Variables'', MS&T15-Materials Science and Technology 2015 Conference, Columbus, Ohio, October 4-8, 2015.
4. Jha, R., Dulikravich, G.S., Colaco, M.J., Fan, M., Schwartz, J. and Koch, C.C., "Magnetic Alloys Design Using Multi-Objective Optimization", ACEX2015-9th International Conference on Advanced Computational Engineering and Experimenting, Munich, Germany, June 29 – July 2, 2015.
5. Jha, R., Dulikravich, G.S., Chakraborti, N., Fan, M., Schwartz, J., Koch, C.C., Colaco, M.J., Poloni, C., Egorov, I.N., "Algorithms for Design Optimization of Hard Magnetic Alloys Using Experimental Data", ICMM4-International Conference on Material Modeling, Berkeley, CA, May 27-29, 2015.
6. Jha, R., Dulikravich, G.S., Fan, M., Schwartz, J., Koch, C., Egorov, I.N., Poloni, C., "A Combined Computational-Experimental Approach to Design of High-Intensity Permanent Magnetic Alloys", CONEM214- *National Congress of Mechanical Engineering* (eds: Steffen, V., Bandarra, E., Rade, D.A.), Uberlandia, Brazil, August 10-15, 2014.
7. Pasqualette, M.A, Colaco, M.J., Dulikravich, G.S. and Orlande, H.R.B., "Inverse Determination of Spatially Varying Diffusion Coefficient in Two-Dimensional Objects, *7th International Conference Inverse Problems: Modeling & Simulation*, Oludeniz, Fethiye, Turkey, May 26-31, 2014.
8. Jha, R., Pettersson, F., Saxen, H., Dulikravich, G.S., Chakraborti, N., "A Combined Experimental-Computational Approach to Design Optimization of High Temperature Alloys", paper no. ETS2014-1008, ASME Symposium on Elevated Temperature

Application of Materials for Fossil, Nuclear, and Petrochemical Industries, Seattle, WA, March 25-27, 2014.

9. Dulikravich, G.S. and Colaco, M.J., "Hybrid Optimization Algorithms and Hybrid Response Surfaces", *Plenary Lecture*, EUROGEN2013, (eds.: Greiner, D., Galvan, B., Periaux, J., Gauger, N., Giannakoglou, K., Winter, G.), Las Palmas de Gran Canaria, Spain, October 7-9, 2013.
10. Pasqualette, M.A., Colaco, M.J., Dulikravich, G.S., Orlande, H.R.B. and Martin, T.J., "Inverse Determination of Spatially Varying Thermal Conductivity Based on Boundary Temperature and Heat Flux Measurements", Symposium on Inverse Problems, Design and Optimization-IPDO2013, (eds.: Fudym, O., Battaglia, J.-L.), Albi, France, June 26-28, 2013.
11. Inclan, E.J., Dulikravich, G.S. and Yang, X.-S., "Modern Optimization Algorithms and Particle Swarm Variations", Symposium on Inverse Problems, Design and Optimization-IPDO2013, (eds.: Fudym, O., Battaglia, J.-L.), Albi, France, June 26-28, 2013.
12. Inclan, E.J. and Dulikravich, G.S., "Effective Modifications to Differential Evolution Optimization Algorithm", International Conference on Computational Methods for Coupled Problem in Science and Engineering, (eds.: Idelsohn, S., Papadrakakis, M., Schrefler, B.), Santa Eulalia, Ibiza, Spain, June 17-19, 2013.
13. Inclan, E.J. and Dulikravich, G.S., "A Hybrid Optimization Algorithm with Search Vector Based Automatic Switching", WCSMO - *World Congress of Multidisciplinary Optimization*, (eds.: Kim, N.-H., Haftka, R.), Orlando, FL, May 15-19, 2013.

Journal papers in print and in the review process acknowledging the AFOSR grant FA9950-12-1-0440 support:

1. Jha, R., Dulikravich, G.S, Colaco, M.J., Fan, M., Schwartz, J. and Koch, C., "Magnetic Alloys Design Using Multi-Objective Optimization", Advanced Structured Materials series (eds.: Oechsner, A., da Silva, L.M., Altenbach, H.), Springer, Germany (http://www.springer.com/series/8611). In print.
2. Dulikravich, G.S., Reddy, S.R., Pasqualette, M.A., Colaco, M.J., Orlande, H.R.B. and Coverston, J., "Inverse Determination of Spatially Varying Material Coefficients in Solid Objects", *Journal on Inverse and Ill-Posed Problems*. In print.
3. Jha, R., Dulikravich, G.S., Chakraborti, N., Fan, M., Schwartz, J., Koch, C., Colaco, M.J., Poloni, C. and Egorov, I.N., "Algorithms for Design Optimization of Hard Magnetic Alloys Using Experimental Data", submitted to *Journal of Alloys and Compounds*.
4. Fan, M., Liu, Y., Jha, G.S., Schwartz, J. and Koch, C.C., "Effect of Cu-Ni-rich Bridges on the Microstructure and Magnetic Properties of AlNiCo Alloys", to be submitted.

List of presentations acknowledging the AFOSR grant FA9550-12-1-0440 support:

2. Jha, R., Dulikravich, G.S., Colaco, M.J., "Design and Optimization of Magnetic Alloys and Nickel-Based Superalloys for High Temperatures Applications", COBEM-2015, paper 1284, Rio de Janeiro, Brazil, December 6-11, 2015.
3. Jha, R., Dulikravich, G.S., Colaco, M.J., Egorov. I.N., Poloni, C., Chakraborti, N., Fan, M., Schwartz, J.and Koch, C.C., "Multi-Objective Design and Optimization of Hard Magnetic Alloys Free of Rare Earths", MS&T15-Materials Science and Technology 2015 Conference, Columbus, Ohio, October 4-8, 2015.
4. Dulikrvich, G.S., Reddy, S., Orlande, H.R.B. and Colaco, M.J., "Inverse Determination of Diffusion Coefficients in Arbitrary Objects Creating Desired Non-isotropy of Field

Variables'', MS&T15-Materials Science and Technology 2015 Conference, Columbus, Ohio, October 4-8, 2015.

5. Jha, R., Dulikravich, G.S., Colaco, M.J., Fan, M., Schwartz, J. and Koch, C.C., "Magnetic Alloys Design Using Multi-Objective Optimization", ACEX2015-9th International Conference on Advanced Computational Engineering and Experimenting, Munich, Germany, June 29 – July 2, 2015.
6. Dulikravich, G.S., Multi-Objective Design Optimization of Arbitrary Alloys including Magnetic Alloys, Dept. of Mechanical Eng., University of Belgrade, Belgrade, Serbia, June 24, 2015.
7. Dulikravich, G.S., Multi-Objective Design Optimization of Arbitrary Alloys including Magnetic Alloys, Dept. of Materials Science, Institut Jozef Stefan, Ljubljana, Slovenia, June 18, 2015.
8. Jha, R., Dulikravich, G.S., Chakraborti, N., Fan, M., Schwartz, J., Koch, C.C., Colaco, M.J., Poloni, C., Egorov, I.N., "Algorithms for Design Optimization of Hard Magnetic Alloys Using Experimental Data", ICMM4-International Conference on Material Modeling, Berkeley, CA, May 27-29, 2015.
9. Jha, R., Dulikravich, G.S., Fan, M., Schwartz, J., Koch, C., Egorov, I.N., Poloni, C., "A Combined Computational-Experimental Approach to Design of High-Intensity Permanent Magnetic Alloys", CONEM214- *National Congress of Mechanical Engineering* (eds: Steffen, V., Bandarra, E., Rade, D.A.), Uberlandia, Brazil, August 10-15, 2014.
10. Pasqualette, M.A, Colaco, M.J., Dulikravich, G.S. and Orlande, H.R.B., "Inverse Determination of Spatially Varying Diffusion Coefficient in Two-Dimensional Objects, *7th International Conference Inverse Problems: Modeling & Simulation*, Oludeniz, Fethiye, Turkey, May 26-31, 2014.
11. Jha, R., Pettersson, F., Saxen, H., Dulikravich, G.S., Chakraborti, N., "A Combined Experimental-Computational Approach to Design Optimization of High Temperature Alloys", paper no. ETS2014-1008, ASME Symposium on Elevated Temperature Application of Materials for Fossil, Nuclear, and Petrochemical Industries, Seattle, WA, March 25-27, 2014.
12. Dulikravich, G.S., "Material Design Methods Based on Multi-Objective Optimization, Inverse Design and Molecular Multi-Functionality", CAVS, Mississippi State University, Starkville, MS, October 31, 2013.
13. Dulikravich, G.S. and Colaco, M.J., "Hybrid Optimization Algorithms and Hybrid Response Surfaces", *Plenary Lecture*, EUROGEN2013, (eds.: Greiner, D., Galvan, B., Periaux, J., Gauger, N., Giannakoglou, K., Winter, G.), Las Palmas de Gran Canaria, Spain, October 7-9, 2013.
14. Pasqualette, M.A., Colaco, M.J., Dulikravich, G.S., Orlande, H.R.B. and Martin, T.J., "Inverse Determination of Spatially Varying Thermal Conductivity Based on Boundary Temperature and Heat Flux Measurements", Symposium on Inverse Problems, Design and Optimization-IPDO2013, (eds.: Fudym, O., Battaglia, J.-L.), Albi, France, June 26-28, 2013.
15. Inclan, E.J., Dulikravich, G.S. and Yang, X.-S., "Modern Optimization Algorithms and Particle Swarm Variations", Symposium on Inverse Problems, Design and Optimization-IPDO2013, (eds.: Fudym, O., Battaglia, J.-L.), Albi, France, June 26-28, 2013.

16. Inclan, E.J. and Dulikravich, G.S., "Effective Modifications to Differential Evolution Optimization Algorithm", International Conference on Computational Methods for Coupled Problem in Science and Engineering, (eds.: Idelsohn, S., Papadrakakis, M., Schrefler, B.), Santa Eulalia, Ibiza, Spain, June 17-19, 2013.
17. Inclan, E.J. and Dulikravich, G.S., "A Hybrid Optimization Algorithm with Search Vector Based Automatic Switching", WCSMO - *World Congress of Multidisciplinary Optimization*, (eds.: Kim, N.-H., Haftka, R.), Orlando, FL, May 15-19, 2013.

Ph.D. Dissertations Completed During These Three Years

1. Rajesh Jha: "Combined Computational-Experimental Design of High Temperature, High Intensity Permanent Magnetic Alloys With Minimal Addition of Rare Earth Elements", May 2016.